Russian Geology and Geophysics © 2019, V.S. Sobolev IGM, Siberian Branch of the RAS
Vol. 60, No. 5, pp. 514–531, 2019 DOI:10.15372/RGG2019028 *Geologiya i Geofizika*

Gold-Bearing Pyrrhotite Ores in East Sayan: Composition and Formation Conditions (by the Example of the Ol'ginskoe Ore Occurrence)

B.B. Damdinov [a, ✉], L.B. Damdinova [a], S.M. Zhmodik [b], A.G. Mironov [a]

[a] *Geological Institute, Siberian Branch of the Russian Academy of Sciences, ul. Sakh'yanovoi 6a, Ulan Ude, 670047, Russia*

[b] *V.S. Sobolev Institute of Geology and Mineralogy, Siberian Branch of the Russian Academy of Sciences, pr. Koptyuga 3, Novosibirsk, 630090, Russia*

Received 16 November 2017; received in revised form 4 March 2018; accepted 25 April 2018

Abstract—We present results of study of the chemical composition, formation conditions, and genesis of gold-bearing pyrite–pyrrhotite ores widespread within the ophiolite belts in the southeast of East Sayan. The study was performed at the Ol'ginskoe ore occurrence localized in the Ol'gino gold ore zone. Sulfide mineralization zones are composed of lenticular interbeds and bodies subconformable with the bedding of the enclosing schist strata. The ores are carbonaceous siliceous garnet–biotite schists variably enriched in sulfide minerals, mainly pyrrhotite, with impurities of other silicate minerals: tremolite, chlorite, albite, plagioclase, diopside, and epidote. In addition, sphalerite, chalcopyrite, pyrite, and arsenopyrite are present in small amounts in the ores. The established *P–T* conditions of ore metamorphism (T = 430–540 ºC, P ~ 5 kbar) correspond to the lower boundary of the epidote–amphibolite facies. Thermobarogeochemical studies of fluid inclusions in vein quartz showed close temperatures (536–340 ºC) but lower pressures, 200–800 bars, which indicates that the quartz vein formation was related to a pressure drop. The predominant salts of the fluid inclusions are Fe and Mg chlorides with Na and K impurities. The geologic location, structures, textures, and mineral, geochemical, and isotope compositions of the studied sulfide ores indicate their formation in submarine deep-water environments as a result of the activity of hydrothermal systems, analogues of "black smokers", later subjected to metamorphism. During metamorphism, primary ores underwent mineral and chemical transformations: pyrrhotitization of pyrite, appearance and coarsening of native gold particles, and redistribution of components (Mn, As, etc). The low contents of gold and some ore-forming elements (Zn, Cu, and Pb) in pyrrhotite ores testify to the removal of these elements with a metamorphogenic fluid. The removed ore-forming components might have been a source of material for later gold–sulfide–quartz deposits of the Urik–Kitoi zone in East Sayan.

Keywords: gold, pyrrhotite ores, composition, formation conditions, genesis, East Sayan

INTRODUCTION

In the southeast of East Sayan, variably metamorphosed schists of a volcanosedimentary part of the ophiolite complex (Ospa Formation, or Il'chir unit) host gold-bearing sulfide (mostly pyrrhotite) mineralization. Fragments and relics of similar pyrrhotite ores were found in many gold–sulfide–quartz deposits in this region, but their role in the mineralization is unclear. Fragments of massive pyrrhotite ores also occur as relics in mineralized zones of the regional largest Zun-Kholba gold deposit or, seldom, form individual bodies. According to the earlier research (Mironov and Zhmodik, 1999; Roshchektaev et al., 2000; Zhmodik et al., 2008), these ores compose an early ore paragenesis formed at the oceanic stage of the deposit evolution. They are the primary gold-bearing substrate that was later transformed to a large deposit.

Many issues of the composition and genesis of pyrrhotite ores localized in schist strata in southeastern East Sayan remain unsolved. In particular, the *P–T* conditions of the ore formation have not been determined, the influence of metamorphism has not been assessed, and the mineral and chemical compositions of the ores, the contents of gold, the regularities of its distribution, and the fluid regime have been poorly studied. One of the controversial problems is the genesis of sulfide mineralization. Earlier it was assumed that the sulfide ores are of submarine hydrothermal-sedimentary nature (Mironov et al., 1999), but the environments and conditions of their formation remain unclear. At the same time, the interest in such sulfide bodies is explained by their possible practical value and by the need of solving a number of scientific problems, namely, elucidation of the prerequisites for the formation of sedimentary strata with a siderophile–chalcophile geochemical specialization, the geodynamic and physicochemical conditions of formation of deposits initially enriched in sulfide minerals, the behavior of gold and ore-forming components during metamorphism, the origin and

✉ Corresponding author.
E-mail adress: damdinov@mail.ru (B.B. Damdinov)

composition of metamorphogenic fluids, and the evolution of the composition of submarine sulfide ores during metamorphism caused by accretion–collision events in the region (Vikent'ev, 2004; Bogdanov et al., 2006; Zhmodik et al., 2006; Nemerov et al., 2010; Budyak et al., 2016). To solve these problems, we studied pyrite–pyrrhotite ores from the Ol'ginskoe gold ore occurrence localized in the Ol'gino gold ore zone of the Oka ore district (Gordienko et al., 2016).

METHODS

The field works at the Ol'ginskoe gold ore occurrence included geological observations of the relationship between sulfide bodies and the host schists and trench and chip sampling.

The contents of major and impurity elements, gold, and silver in rocks and ores were determined by AAS, XRF, chemical spectral, and ICP AES analyses at the Geological Institute, Ulan Ude (analysts B.Zh. Zhalsaraev, A.A. Tsyrenova, B.B. Lygdenova, L.A. Levantueva, L.V. Mitrofanova, O.V. Korsun, M.G. Egorova, and I.V. Zvontsov). The isotope compositions of sulfur and oxygen were studied at the Institute of Geology and Mineralogy, Novosibirsk (analyst V.A. Ponomarchuk), and at the Geological Institute, Ulan Ude (analysts V.F. Posokhov and V.L. Posokhova), respectively.

The thin and polished sections of rocks were examined using Olympus BX-51 and Polam P-312 polarizing microscopes. The chemical composition of ore minerals was studied on a Leo-1430 scanning electron microscope with an Inca-Energy 350 microprobe at the Geological Institute, Ulan Ude (analysts S.V. Kanakin and E.A. Khromova).

Fluid inclusions (FI) in quartz and siderite were investigated by the thermometric and cryometric methods. The temperatures of total homogenization, eutectics, and melting of ice of aqueous solutions and the temperatures of partial homogenization and melting of liquefied gases were measured on a Linkam THMSG-600 thermal microstage with a temperature range from –196 to 600 ºC. The standard instrumental error of measurement was ±0.1 ºC in the range of negative temperatures and ±5 ºC in the range of positive temperatures. The total salinity of aqueous solutions in FI was evaluated from the dissolution temperature of halite daughter crystal (Bodnar and Vityk, 1994). The predominant salts in the aqueous solution of FI were determined from the eutectic temperature, a marker of the water–salt system (Borisenko, 1977).

THE OL'GINO GOLD ORE ZONE

Data on the geologic structure, geodynamic evolution, and metallogeny of the study region are given in many publications (Belichenko et al., 1988; Dobretsov et al., 1989; Fedotova and Khain, 2002; Kuzmichev, 2004, 2015; Zhmodik et al., 2006; Gordienko et al., 2016). The Ol'gino gold ore zone is part of the Bokson–Gargan structure-metallogenic zone and borders upon the Urik–Kitoi gold ore zone and the Ospa ore cluster. The Ol'gino zone stretches along the northern boundary of the Ospa–Kitoi ultrabasic massif and comprises a number of same-type gold ore occurrences (Ol'ginskoe, Barun-Ospa, Veresen', Sentyabr'skoe, etc.) localized in metamorphosed volcanosedimentary deposits of an ophiolite complex in the southeast of East Sayan. These deposits are subjected to plicate and disjunctive deformations, such as folding, foliation, and fracturing. Primary rocks were metamorphosed to schists of different compositions with intercalates of amphibolites and siliceous rocks and, seldom, with carbonate olistoliths.

The ophiolites under study form the two largest belts, Il'chir (southern) and Bokson–Kharanur (northern), framing the Gargan block (an uplift of the basement of the Tuva–Mongolian paleomicrocontinent) on both sides (Fig. 1). On the eastern intersection of the two belts, there is the regional largest Ospa–Kitoi ultrabasic massif. These ophiolite belts are considered to be relics of the Dunzhugur island arc (Kuzmichev and Larionov, 2013). The ophiolite blocks have an intricate nappe–scaly structure and include (mostly as fragments) all members of the ophiolite rock association: restitic ultrabasic rocks, layered rocks of a cumulative complex, basic dikes, gabbroids, and metamorphosed volcanosedimentary rocks (Dobretsov et al., 1985; Kuzmichev, 2004). There are usually three "scales" (plates) within the ophiolite nappe: upper ultrabasic, middle, composed of rocks of banded and gabbro complexes, and lower volcanosedimentary. This plate sequence indicates a reverse bedding of ophiolites. The basements of all ophiolite nappes have zones of serpentinite melange or melange–olistostrome complex as well as plates composed of rocks of the Ospa Formation (carbonaceous siliceous schists, metamorphosed volcanosedimentary rocks).

The ophiolites under study are the oldest in the Central Asian Orogenic Belt, >1035 Ma. The dates of 1022 and 1035 Ma were obtained for zircons from plagiogranites and metaeffusive rocks associated with ophiolites of the Dunzhugur ultrabasic–basic massif (nappe) (Khain et al., 2002; Kuzmichev and Larionov, 2013). The age of the obduction of ophiolite blocks (accretion of the Dunzhugur island arc to the Gargan continental block) is estimated at ~800 Ma (Kuzmichev, 2004).

Stratigraphically, the schist bed with sulfide bodies belongs to the Il'chir unit or the Ospa Formation.

The Il'chir unit is composed of volcanosedimentary deposits, including altered greenstone basalts and andesites intimately associated with foliated tuffs and tuffites as well as scarcer carbonaceous siliceous and carbonaceous clay schists alternating with sandstones and siltstones. The effusive rocks are metamorphosed up to green schists. Locally, olistostromes are present. Their matrix is formed mostly by green and dark gray phyllite-like (sometimes, carbonate) schists, often containing sulfides. Olistoliths and olistoplaques are composed of limestones, carbonate schists, talc–

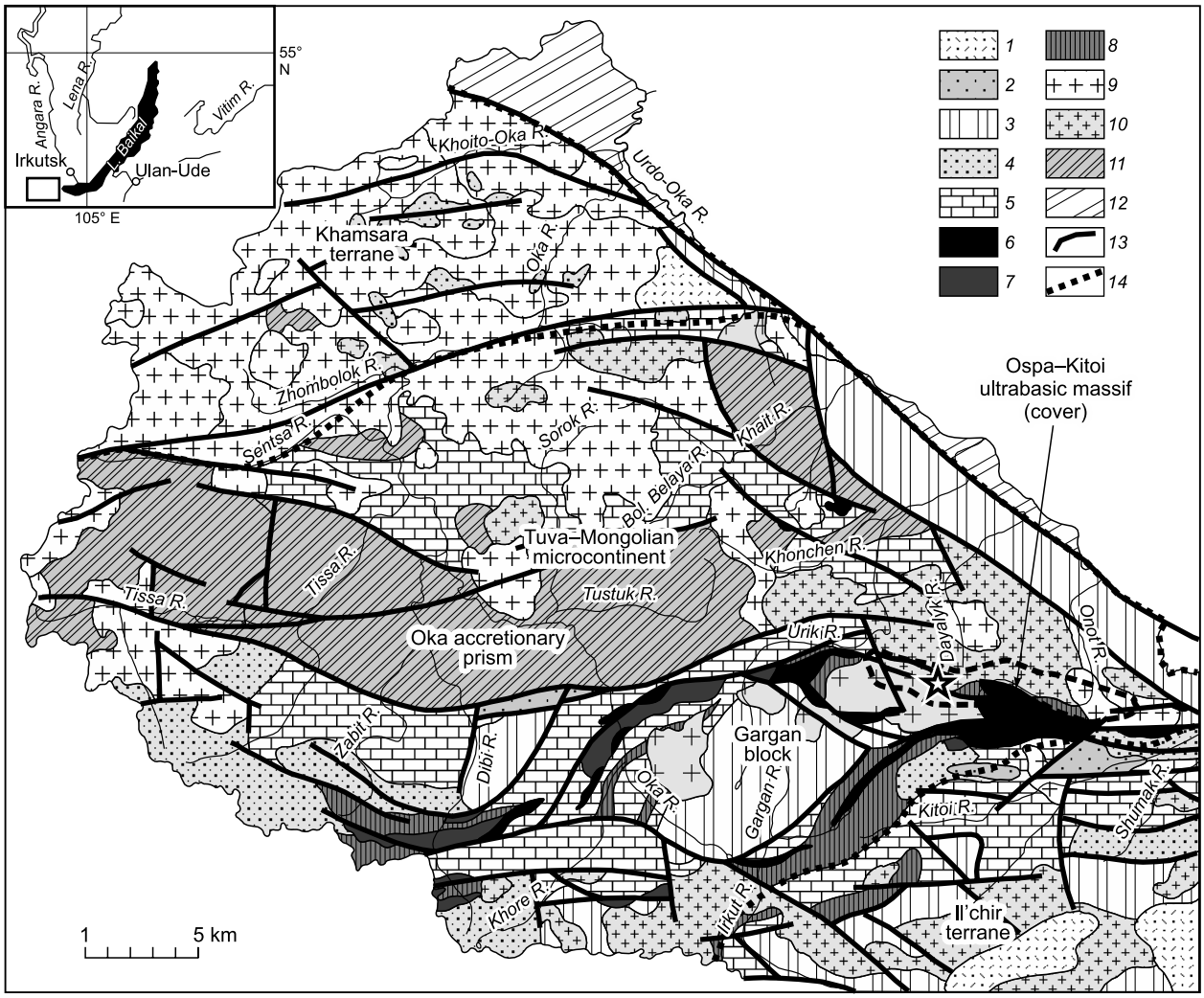

Fig. 1. Schematic map of the geologic and tectonic structure of southeastern East Sayan, compiled after V.P. Arsent'ev, V.G. Belichenko, L.S. Volkov, V.F. Volkolakov, P.V. Dubin, V.I. Pelepyagin, V.V. Levitskii, A.L. Samburg, G.K. Takaishvili, G.A. Gusarevich, and A.B. Kuzmichev. *1*, *2*, continental-molassa associations: *1*, carbonaceous (Narin-Gol Formation, Gusinoe Ozero Group, MZ) (Tunka depression), *2*, variegated (Sagansair Formation, PZ_2); *3–5,* Tuva–Mongolian microcontinent: *3*, crystalline basement (granite-gneisses and amphibolites), *4*, volcanic association (Ilei unit, Sarkhoi Formation); *5*, carbonate association (Bokson Group, Mongosha and Irkut Formations); *6–8*, ophiolite complex: *6*, ultrabasic rocks, *7*, basic rocks, *8*, volcanosedimentary and black-schist deposits (Dibi and Ospa Formations, Il'chir unit); *9*, Paleozoic intrusions; *10*, Proterozoic intrusions; *11*, deposits of the Oka accretionary prism (Oka Group, Bilin Formation); *12*, Siberian Platform basement; *13*, faults; *14*, terrane boundaries. Dash line outlines the Ol'gino gold ore zone, asterisk marks the location of the Ol'ginskoe ore occurrence.

carbonate rocks, ultrabasic rocks, and, sometimes, diabases and gabbro, i.e., members of the ophiolite association. They are in tectonic contact with the underlying carbonate unit (Irkut Formation).

The Ospa Formation comprises volcanosedimentary deposits of the upper plate of the ophiolite association and the deposits that were earlier assigned to the Il'chir, Daban-Zhalga, Dibin, and Dunzhugur Formations. The Ospa Formation is composed of predominant metabasalts and metaandesites and subordinate dark gray and green schists with intercalates of siliceous and carbonate rocks, sandstones, and siltstones. There are also local sites with an ophiolitoclastic olistostrome.

As seen from the above short description, both stratigraphic units are made up of compositionally similar metamorphosed volcanosedimentary deposits spatially associated with the ophiolite rocks. For this reason, the separation of the Il'chir unit and the Ospa Formation is still uncertain. According to Kuzmichev (2004), there are no clear lithological criteria for distinguishing between the Ospa and Il'chir Formations. At the same time, there are gradual transitions from the Irkut Formation composing the cover of the Tuva–Mongolian microcontinent to the Il'chir Formation (Belichenko et al., 1988). Probably, the Il'chir unit includes both the cover sediments and the deep-water sediments and effusive deposits of the ophiolite association that should be

referred to as the Ospa Formation. However, the nature of the Ospa Formation (ophiolite plate) and the Il'chir unit (cover sediments) and their relationship are still unclear, because there are no reliable criteria for their separation.

The schist strata under study are coeval with the ophiolites (>800 Ma), as evidenced from their intrusion by granitoids of the Sumsunur complex (790 Ma). The earlier Rb–Sr dating of sulfidized carbonaceous schists from the upper ophiolite plate, sampled within the Zun-Kholba gold deposit, yielded the age of metamorphism of 709 Ma (Posokhov et al., 1994). This date is close to the age of obduction of ophiolite blocks.

Schists of the Ol'gino gold ore zone are highly metamorphosed, which is expressed as the presence of biotite and garnet and the appearance of amphibolites. There are almost no volcanosedimentary rock structures; primary rocks are metamorphosed into carbonaceous siliceous schists with intercalates of amphibolites and garnet–biotite and siliceous chlorite–tremolite schists. The rock schistosity is conformable with the ore zones, which are horizons of continuous and disseminated sulfide mineralization. The ore mineralization is slightly dependent on the lithologic composition of the rocks. In particular, the sulfide bodies are enriched in carbonaceous material, whereas the host strata are poor in carbonaceous schists. Pyrite mineralization is observed throughout the strata section, being most abundant in its middle part. Scarce quartz veins and lenses occur subconformably with the host rocks and also in fractures, being in cutting contact with the latter. Quartz veins are also localized near the schist strata contacts, in particular, at the exocontact of limestone strata, e.g., in the Podkova and Veresen' ore occurrences. Gold-bearing sulfide–quartz veins occur either at the strata contacts or in limestones near the strata contact with schists. The sulfidized schists are also gold-bearing, Au = 0.8–16 ppm (unpublished data by A.P. Osokin).

THE OL'GINSKOE ORE OCCURRENCE: GEOLOGIC STRUCTURE AND ROCK COMPOSITION

The ore occurrence is localized in the upper course of the Dayalyk River (a right tributary of the Urik River), on both slopes of its valley in the interfluve of the uppermost tributaries. It is confined to a narrow band of metamorphosed volcanosedimentary deposits of the Ospa Formation, stretching to the southeast from the valley of the Ambarta-Gol River (a right tributary of the Urik River) to the upper course of the Onot River (the northern margin of the Ospa–Kitoi ultrabasic massif). Thus, the ore occurrence is only a minor fragment of the Ol'gino zone. In the north and in the south, this site is bounded by granitoid massifs assigned to the Sumsunur intrusive complex and is 1.1–1.2 km wide. The southern contact of the schist strata is tectonic, complicated by mylonitization of granitoids, and the northern contact is intrusive. The area of the Ol'ginskoe ore occurrence is composed of quartz–biotite and quartz–amphibole–biotite schists with garnet (1–7%), carbonaceous material (0.1–2.5%), and pyrrhotite (0.5–3.5%) and of siliceous (quartzite-like) and carbonaceous siliceous rocks (lydites), with subconformable low-sulfide quartz veins localized among them (Fig. 2). Some bodies are formed by amphibole rocks with disseminated pyrrhotite mineralization.

Sulfide ore zone extends for about 4 km from east to west and is 20 to 40 m thick. Its western flank is cut by NE striking fault, along which granites of the northern field make contact with schists. In the east, the zone is overlain by loose deposits of the Dayalyk–Barun-Ospa watershed. The eastern and central segments of the zone are localized in a member of carbonate–quartz–biotite schists, and the western segment lies in quartz–chlorite–amphibole schists. Thus, the ore zone has a discordant structure, crossing the contact of the mentioned two members at an acute angle. Sulfide ores are conformable with schistosity in the section. In the central part of the zone they are of subvertical occurrence or steeply dip in the S–SW direction.

On the hanging flank of the sulfidization zone, schists alternate with amphibolites with quartzite intercalates (Fig. 3). The schists are dark gray and have siliceous biotite–garnet–tremolite and siliceous tremolite–garnet compositions. Quartz amounts to ~60 vol.%. It composes continuous bands, lenses, and oriented aggregates of fine (0.01–0.20 mm) grains of irregular shape, pure or slightly pigmented with carbonaceous material. Tremolite (8–20 vol.%) and biotite (5 vol.%) form bimineral lenticules and bands. In addition, tremolite, together with quartz, forms bands of nematoblastic texture. Garnet (10 vol.%) occurs as porphyroblasts 0.2–2.0 mm across (often with traces of corrosion, shearing, and destruction) in quartz and amphibole–biotite matrix, which often envelopes garnet grains, forming a microaugen structure.

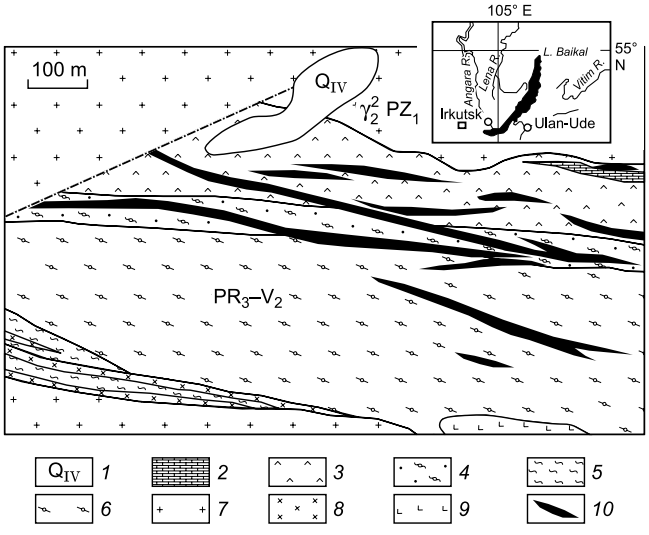

Fig. 2. Schematic geologic structure of the Ol'ginskoe ore occurrence (Mironov and Zhmodik, 1999). *1*, Quaternary deposits; *2*, limestones; *3*, quartz–chlorite–amphibole schists; *4*, quartz–garnet–biotite schists; *5*, garnet–carbonate–mica schists; *6*, garnet–amphibole–biotite schists; *7*, plagiogranites; *8*, diorites; *9*, ultrabasic rocks; *10*, sulfide bodies. Dash-dot line marks fault.

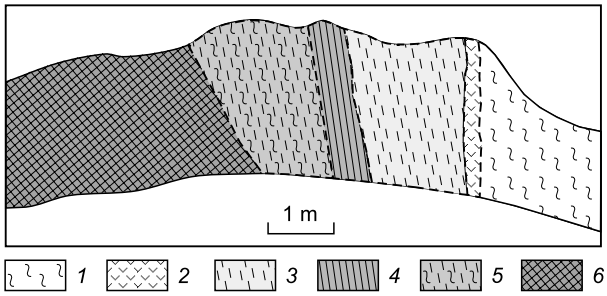

Fig. 3. Fragment of a section of the schist strata hosting a sulfide body (compiled after A.G. Mironov). *1*, siliceous garnet–biotite–sericite schists; *2*, amphibolites; *3*, siliceous garnet–biotite–amphibole schists with quartzite intercalates; *4*, crushing zone; *5*, banded siliceous garnet–biotite–amphibole schists with amphibolite intercalates; *6*, sulfide ores (carbonaceous siliceous biotite–garnet–tremolite schists with pyrrhotite).

There is also the second generation of garnet in the form of fine grains (0.01–0.05 mm) forming chains and aggregates around large resorbed porphyritic garnet crystals. Sometimes, chains of younger garnet intersect quartz aggregates.

Amphibolites are dark green, with a plagioclase–biotite–hornblende composition and a fine-banded structure due to alternating discrete mono- and bimineral amphibole and biotite partings. Hornblende (55–56 vol.%) composes tabular and prismatic (0.01–0.20 mm) crystals with elongation oriented along the rock banding. Biotite (25 vol.%) has a similar orientation, except for large porphyroblasts (0.10–0.15 mm) arranged transversely to the rock schistosity and usually replaced by chlorite. Plagioclase (10 vol.%) occurs as transparent tabular-prismatic and isometric grains (0.05–0.10 mm) with thin twinning in the hornblende interstices. Accessory minerals are apatite, sphene, and leucoxene. Ore minerals (sulfides) (5–8 vol.%) form chains and elongate aggregates of finely disseminated structure. Their isometric and scarcer prismatic grains are 0.01–0.05 mm in size. Most aggregates are conformable with the rock banding and are localized at the contacts of plagioclase and biotite–hornblende clusters.

The hanging flank of the sulfidization zone is composed of amphibolites consisting of hornblende with chlorite (3%) and biotite (1%) impurities. Closely packed aggregates of fine-grained hornblende are saturated (11%) with finely disseminated (0.01–0.02 mm) ore mineral. It often forms nests elongated along the rock schistosity. Mineralogical analysis showed that the rock contains pyrrhotite (0.5%), limonite (0.15%), signs of pyrite, magnetite, ilmenite, and apatite (<0.1%), and scarce signs of galena and arsenopyrite. The studied trench sulfide deposit is oxidized from the surface, but to a minor depth (fractions of centimeters). In fresh cleavage, the ore is massive or banded and is composed (30–60%) of pyrrhotite with scarce pyrite and chalcopyrite inclusions, single arsenopyrite crystals, and thin dark gray carbonaceous essentially quartz aggregates with finely disseminated ore minerals. In places, clastic aggregates are observed (Fig. 4*a*). West of the pyrite ore outcrops, biotite–amphibole schists bear a 0.5 m thick quartz vein dipping at 45–50º to the north. Its total length is unknown. Quartz crystals are transparent yellowish (because of the penetration of iron hydroxides into their cracks) and coarse. Quartz veins are extremely poor in sulfide minerals in contrast to the host schists saturated with them (Fig. 4*b*). There are occasional pyrrhotite veinlets, phenocrysts, and nests (up to 3–5 cm across) near the quartz grain selvages.

ORE COMPOSITION

Mineral composition of ores. Mineral analysis showed that the sulfide bodies are composed of pyrrhotite (26.50–77.92 vol.%) and a carbon–silicate aggregate (4.77–73.20 vol.%). Other ore minerals are pyrite (from scarce signs to 0.6 vol.%), arsenopyrite (from scarce signs to

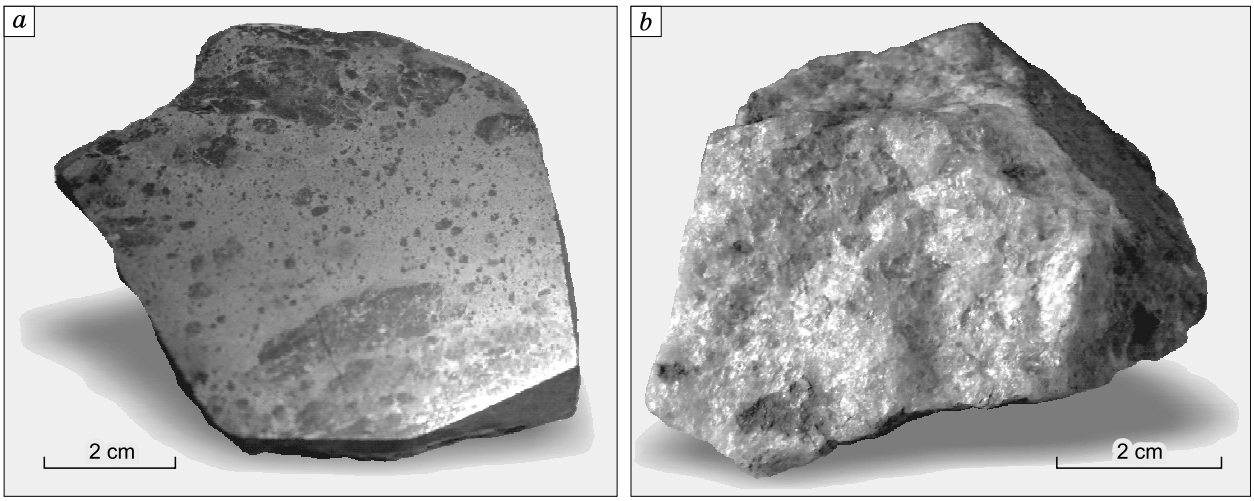

Fig. 4. Photographs of the samples: *a*, massive fine-grained pyrrhotite ore with numerous ovoids of dark quartz and carbonaceous flints (siliceous schists), the sample edges have a brecciform structure; *b*, vein quartz.

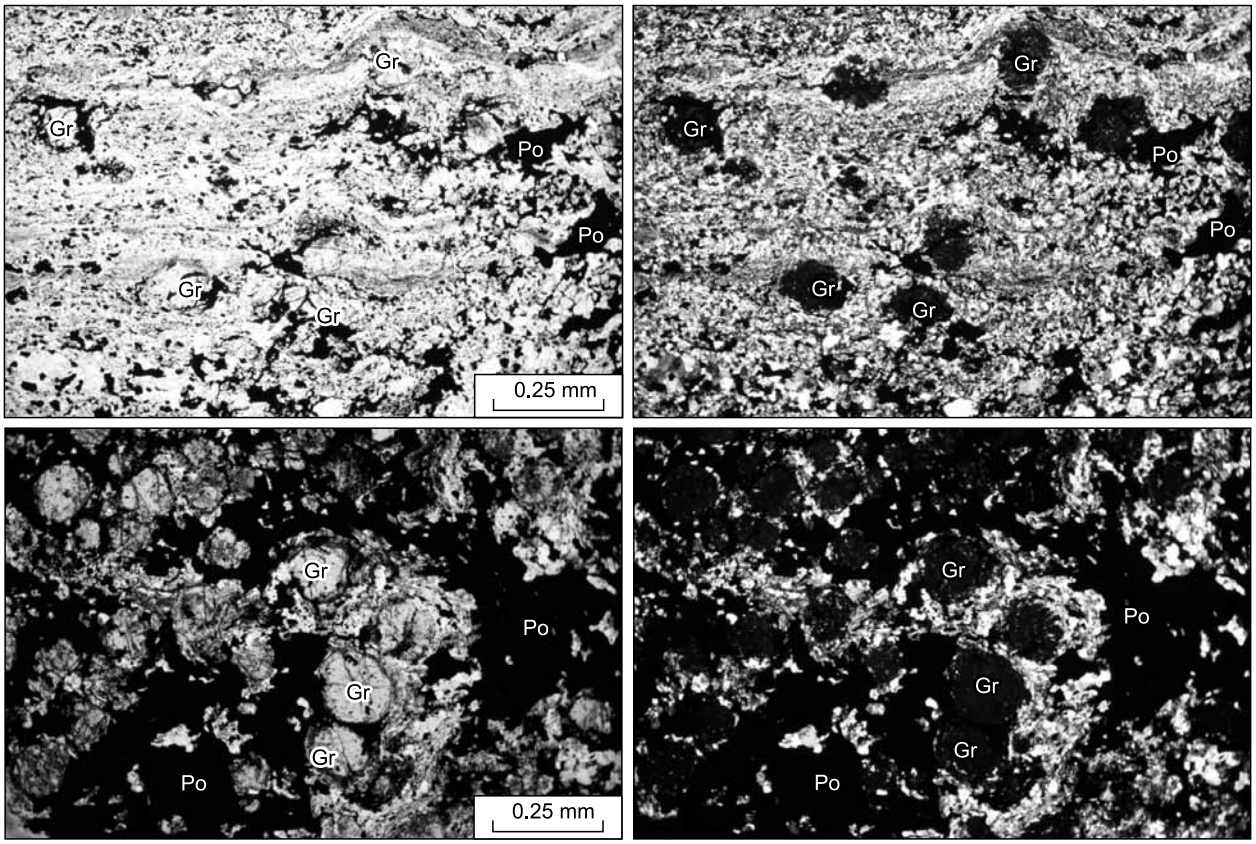

Fig. 5. Photographs of thin sections of sulfidized schists (left, in one nicol; right, with an analyzer). The rock groundmass is composed of fine-grained quartz–biotite aggregate with impurities of amphiboles and other minerals. Gr, garnet, Po, pyrrhotite.

<0.1 vol.%), sphalerite, and galena (from scarce to a few signs). Chalcopyrite (from scarce signs to a few signs) was detected in three samples. Limonite and other iron hydroxides amount to ≤0.5 vol.%. Amphibole, pyroxenes, chlorite, biotite, and garnet are present ubiquitously as an impurity. The hanging side of the body contains scarce signs of Mn mineral, ilmenite, and apatite.

Microscopic examination of the ores showed that they are composed of sulfide-saturated carbonaceous siliceous biotite–garnet schists with impurities of tremolite, chlorite, epidote, and muscovite and of minor diopside, plagioclases, K–Na-feldspars, chlorite, and epidote (Fig. 5). There is also REE-enriched epidote. Accessory minerals are monazite, apatite, rutile, titanite, and zircon. Major minerals are present in varying proportions.

Garnet corresponds in composition to spessartine $(Mn_{2.482}Ca_{0.248}Mg_{0.196}Fe_{0.163})_{3.089}Al_{1.911}(Al_{0.043}Si_{2.957})_3O_{12}$.

A specific feature of the studied minerals is a permanent impurity of Mn in diopside, biotite, tremolite, muscovite, and chlorite:

diopside — $Ca_{0.955}(Mg_{0.873}\mathbf{Mn_{0.072}}Fe^{2+}_{0.073}Fe^{3+}_{0.013})_{1.031}(Al_{0.027}Si_{1.973})_2O_6$;

tremolite — $(Ca_{1.801}\mathbf{Mn_{0.093}})_{1.894}(Mg_{4.205}Fe^{2+}_{0.212}Fe^{3+}_{0.38}\mathbf{Mn_{0.19}}Al_{0.0012})_{1.031}(Fe^{3+}_{0.045}Al_{0.251}Si_{7.704})_8O_{22}(OH)_2$;

biotite — $K_{0.61}(Mg_{2.136}Fe_{0.929}\mathbf{Mn_{0.104}}Ti_{0.081})_{3.25}(Al_{1.297}Si_{2.709})_{4.006}O_{10}(OH)_2$;

muscovite — $K_{1.047}(Al_{1.868}Fe_{0.092}\mathbf{Mn_{0.019}})_{1.979}(A_{l0.88}Si_{3.12})_4O_{10}(OH)_2$;

chlorite (chamosite) — $(Fe_{2.239}Mg_{1.43}\mathbf{Mn_{0.248}}Ca_{0.172}Al_{1.597})(Al_{0.976}Si_{3.024})_4O_{10}(OH)_8$.

The sulfide ores have mostly disseminated, massive, and fluidal banded textures and also bear relics of detrital brecciform textures. Major ore mineral is pyrrhotite, which composes allotriomorphic aggregates of irregular shape, often band-like and oriented in the same direction or fluidal (Fig. 6). Structurally, it is typical monoclinic pyrrhotite with characteristic reflexes d = 2.069 and 2.649. The average calculated crystallochemical formula of the mineral is $Fe_{7.19}S_{7.77}$, which indicates a sulfur deficit.

The pyrrhotite aggregate contains morphologically similar scarce sphalerite and chalcopyrite segregations of irregular elongate shape. Sphalerite is highly ferroan (Fe ≤ 9.8 wt.%). There are also scarce hypidiomorphic pyrite and arsenopyrite metacrysts up to 4–5 mm in size (Fig. 7). Arsenopyrite has impurities of Ni (up to 0.63 wt.%) and Co (up to 2.67 wt.%); S/As = 1.12–1.21. Single uraninite and altaite grains are also identified.

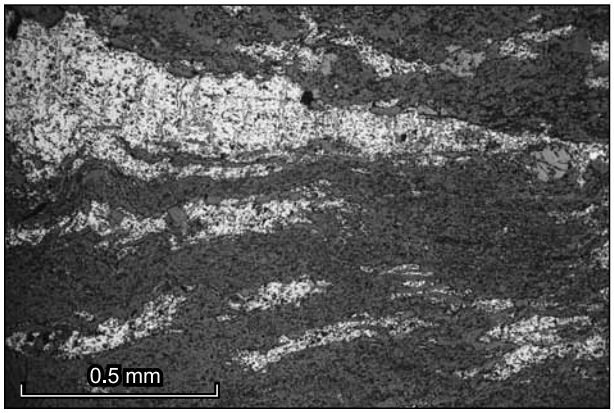

Fig. 6. Fluidal texture of sulfide ore.

Chemical composition of ores. Major ore elements are Fe (up to 41.65 wt.% FeO_{tot}), Si (33.0–55.6 wt.% SiO_2), and S (10.49–17.8 wt.%) (Table 1). The ores have high contents of MnO (0.44–2.63 wt.%) and P_2O_5 (0.35–0.56 wt.%). Few samples contain TiO_2 (up to 2.03 wt.%). The contents of CaO, MgO, and Al_2O_3 vary within a few wt.%.

Sulfidized schists have moderately high contents of impurity elements Cu, Zn, Ni, V, and Cr (few hundred ppm), which are close to their contents in basic igneous rocks. This suggests that the schists formed from volcanosedimentary rocks derived from basaltoids enriched in Fe sulfides and Mn minerals. Compared with the host schists, the sulfide ores are richer in carbonaceous material (C_{org} = 2.6–7.9%), Cu (up to 788 ppm), and Zn (up to 674 ppm). They have impurities of Pb and As, whose contents in the host schists are below the detection limits. Some ore samples are characterized by high Ba contents (up to 666 ppm).

The general trace-element spidergram is similar to that of oceanic-island basalts (OIB) but shows negative Nb, Sr, and Zr anomalies and positive Pb, U, and Ni anomalies (Fig. 8*a*). Such anomalies are typical of suprasubductional basalts of back-arc basins (Metcalf and Shervais, 2008). Wide dispersion of contents is observed for Rb and Ba, large-ion lithophile elements (LILE); it is, most likely, due to secondary alterations of rocks. The REE pattern of sulfide ores is fractionated and demonstrates enrichment in LREE and a distinct negative Eu anomaly (Fig. 8*b*). The LREE pattern is similar to that of OIB but shows higher contents of HREE. This might be the result of metamorphism, which led to the disintegration of primary feldspars (plagioclase) and the formation of garnet accumulating mostly HREE. Monazite and epidote are concentrators of LREE. The REE patterns of the host schists are almost identical to those of OIB (Fig. 8*c*).

The suprasubductional nature of the primary effusive rocks is also evidenced from the Th/Yb–Nb/Yb classification diagram (Fig. 9); these elements are inert during secondary alterations. The composition points of sulfidized schists fall in the field of basalts of back-arc spreading zones.

Isotope compositions of sulfur and oxygen. Isotope composition of sulfur was determined both in sulfides of pyrite bodies from the Ol'gino and Il'chir sites of the Nizhnyaya zone and in sulfides from carbonaceous schists of the Ospa Formation and the Il'chir unit at the Il'chir, Er'e–Khara-Zhalga, and Barun-Gol sites. As seen from Table 2, sulfides from pyrite bodies differ strongly in isotope composition from sulfides disseminated throughout the schist unit. The isotope composition of sulfur in ore sulfides is within 0.5–5‰ and is similar to that in gold deposits of the Urik–Kitoi zone in East Sayan (Mironov and Zhmodik, 1999; Zhmodik et al., 2008). Sulfides from present-day and ancient hydrothermal systems of oceanic and back-arc spreading zones ("black smokers") have the same isotope composition of sulfur (Vikent'ev, 2004; Bogdanov et al., 2006; Seal, 2006). Dispersed sulfides are characterized by negative $\delta^{34}S$ values, from –8.4 to –21.5‰. This isotope composition corresponds to isotopically light sedimentary sulfur (Faure, 1986).

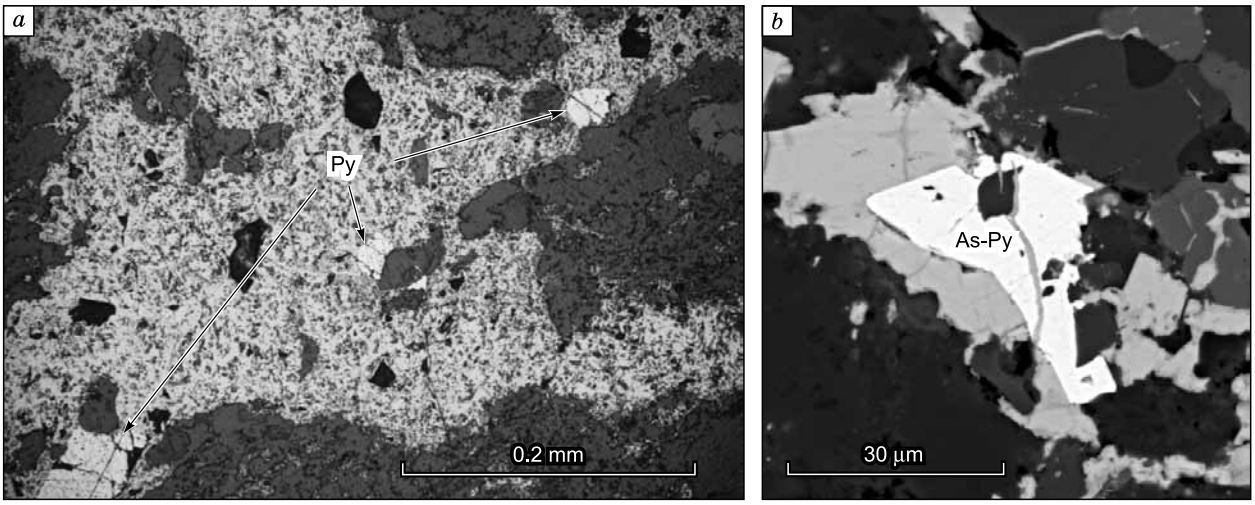

Fig. 7. Pyrite (*a*) and arsenopyrite (*b*) metacrysts in pyrrhotite aggregate. Py, pyrite, As-Py, arsenopyrite.

Table 1. Chemical composition of rocks and ores

Component	d-10	d-14	d-18	d-18b	d-19	d-6	d-96	s-18	d-10b	d-5	d-7	d-2	d-3	d-4	d-4b
	1	2	3	4	5	6	7	8	9	10	11	12	13	14	15
SiO_2, wt.%	55.60	36.30	33.00	33.10	34.20	40.60	36.70	41.30	54.30	52.30	44.40	64.60	44.70	45.50	76.70
TiO_2	0.29	0.13	2.03	0.17	0.22	0.18	0.20	0.14	0.22	0.17	0.19	0.26	3.00	2.09	0.34
Al_2O_3	5.60	2.90	11.80	3.10	4.10	3.80	3.20	3.00	4.60	3.60	4.10	4.40	14.60	9.30	6.10
Fe_2O_3	–	–	–	–	–	–	–	–	–	–	–	6.14	2.19	3.41	1.85
FeO	19.13	36.13	28.73	41.65	40.70	37.06	38.88	33.11	24.71	28.15	34.79	7.38	11.27	9.39	6.70
MnO	1.56	0.85	0.44	0.89	2.63	2.26	0.95	0.99	1.16	1.38	2.29	5.06	0.29	0.29	0.35
MgO	1.86	4.65	5.01	2.95	2.34	2.61	2.97	5.03	2.51	2.37	2.14	4.82	7.04	14.90	1.94
CaO	2.55	5.39	5.09	5.28	2.22	2.82	5.03	6.56	3.03	1.74	2.25	4.12	11.92	11.60	1.51
Na_2O	0.28	0.51	0.49	0.48	0.23	0.22	0.41	0.57	0.27	0.26	0.18	0.08	0.78	0.77	0.87
K_2O	0.76	0.08	3.77	0.87	1.02	0.07	1.01	0.09	0.61	0.39	0.29	0.01	0.14	0.14	0.35
P_2O_5	0.56	0.37	0.35	0.38	0.41	0.44	0.38	0.38	0.55	0.44	0.39	0.14	0.36	0.28	0.85
LOI	11.18	12.28	9.26	11.26	11.46	9.68	10.06	8.68	7.18	8.38	8.14	3.14	2.73	2.46	2.04
Total	99.37	99.57	99.97	100.13	99.53	99.74	99.79	99.85	99.14	99.18	99.16	100.15	99.02	100.13	99.60
S	10.49	14.94	12.17	17.80	16.66	15.39	15.81	13.16	10.99	11.65	14.36	0.23	0.32	0.44	0.23
Ba, ppm	267.0	15.0	666.0	185.0	184.0	24.0	195.0	21.0	158.0	192.0	133.0	23.0	151.0	15.0	120.0
Rb	25.0	3.2	165.0	22.0	29.0	6.2	27.0	5.2	22.0	17.0	12.0	2.3	6.4	3.4	9.0
Sr	118.0	95.0	243.0	144.0	69.0	68.0	157.0	112.0	125.0	52.0	65.0	18.0	362.0	182.0	174.0
Ga	8.1	6.1	20.2	8.0	7.2	4.6	6.8	4.6	9.7	6.0	5.6	6.6	19.1	14.0	10.0
Nb	5.8	2.7	46.0	3.4	5.8	5.0	1.8	2.3	4.0	3.6	3.2	3.4	64.0	36.0	6.3
Hf	4.9	11.7	8.6	B.d.l.	8.7	4.6	5.9	5.8	10.0	7.4	9.3	5.2	10.0	4.0	6.8
Zr	68.0	61.0	141.0	55.0	70.0	55.0	58.0	54.0	51.0	53.0	45.0	69.0	222.0	128.0	66.0
Y	55.9	62.4	62.5	44.4	65.2	69.6	49.0	60.3	35.0	70.0	47.0	92.2	30.0	20.1	40.0
Th	8.7	2.3	2.9	4.5	2.9	5.7	1.5	6.4	4.5	B.d.l.	5.3	B.d.l.	9.5	5.2	7.8
U	B.d.l.	4.9	B.d.l.	4.2	2.4	4.0	4.4	4.1	3.0	3.1	B.d.l.	B.d.l.	B.d.l.	B.d.l.	3.0
Cr	205.0	80.0	290.0	126.0	173.0	300.0	126.0	112.0	167.0	438.0	142.0	180.0	105.0	1103.0	239.0
Ni	215.0	240.0	232.0	384.0	313.0	330.0	252.0	256.0	210.0	240.0	303.0	11.0	102.0	361.0	33.0
Co	45.0	54.0	B.d.l.	94.0	77.0	89.0	58.0	65.0	50.0	39.0	46.0	5.0	57.0	61.0	8.0
Sc	6.4	6.0	32.0	7.0	4.0	3.1	1.7	9.0	4.5	4.6	7.0	7.6	18.3	28.4	8.4
V	275.0	115.0	287.0	140.0	190.0	210.0	152.0	131.0	165.0	265.0	185.0	212.0	285.0	210.0	100.0
Cu	650.0	460.0	580.0	390.0	570.0	660.0	910.0	540.0	890.0	700.0	430.0	94.0	40.0	40.0	540.0
Pb	37.4	11.6	22.6	47.4	15.5	35.8	63.0	9.7	35.7	16.4	31.9	B.d.l.	6.4	B.d.l.	42.2
Zn	325.0	190.0	674.0	199.0	112.0	239.0	493.0	203.0	328.0	224.0	95.0	101.0	117.0	90.0	149.0
Mo	10.0	10.0	2.3	7.9	9.0	B.d.l.	7.0	9.4	11.0	5.8	13.0	4.8	B.d.l.	1.7	B.d.l.
Ag	B.d.l.	2.5	3.5	4.0	3.0	12.0	4.0	B.d.l.	3.2	3.0	9.9	B.d.l.	B.d.l.	B.d.l.	B.d.l.
As	2.4	6.0	1.6	33.0	5.0	B.d.l.	6.3	5.1	B.d.l.	1.3	B.d.l.	2.3	3.0	3.3	B.d.l.
Se	8.6	10.0	6.2	9.0	10.1	B.d.l.	7.2	8.1	4.2	10.0	B.d.l.	3.3	B.d.l.	2.1	B.d.l.
La	34.50	39.10	39.00	41.20	43.00	46.40	–	37.90	–	–	–	4.90	44.20	26.60	–
Ce	58.20	61.70	70.00	78.50	78.50	76.50	–	69.20	–	–	–	8.79	89.20	56.00	–
Pr	8.45	8.50	8.50	9.21	9.60	8.51	–	9.80	–	–	–	B.d.l.	9.21	5.90	–
Nd	33.40	35.30	40.20	38.70	45.00	39.40	–	38.10	–	–	–	6.40	37.40	24.10	–
Sm	8.46	8.47	10.50	9.61	10.90	10.10	–	9.75	–	–	–	2.24	8.82	6.22	–
Eu	1.49	2.12	2.27	2.53	2.49	2.31	–	2.33	–	–	–	1.29	2.54	1.86	–
Gd	8.32	8.88	10.50	8.56	10.60	10.50	–	9.66	–	–	–	7.65	7.02	4.98	–
Tb	1.42	1.35	1.54	1.28	1.56	1.72	–	1.61	–	–	–	1.60	1.00	B.d.l.	–
Dy	8.27	9.38	9.54	7.27	9.66	10.90	–	9.34	–	–	–	11.70	5.35	3.72	–
Ho	1.97	2.23	2.22	1.61	2.32	2.47	–	2.21	–	–	–	2.94	0.98	0.63	–
Er	5.50	6.40	6.33	4.67	6.50	7.25	–	6.37	–	–	–	9.57	2.63	1.66	–
Tm	0.86	0.94	0.89	0.66	0.99	1.03	–	0.94	–	–	–	1.34	0.35	B.d.l.	–
Yb	5.35	5.36	5.23	3.91	5.61	5.96	–	5.15	–	–	–	8.26	2.03	1.35	–
Lu	0.84	0.85	0.84	0.64	0.89	0.94	–	0.83	–	–	–	1.26	0.33	0.23	–

Note. 1–11, sulfide ores (sulfidized carbonaceous siliceous garnet–biotite schists); 12, siliceous garnet–tremolite (actinolite) schist; 13, sericite–albite–actinolite schist; 14, tremolitite with fine chrysotile lenses; 15, siliceous chlorite–garnet–biotite schist. Dash, not determined. B.d.l., below detection limit. In samples 1–11, the total iron content is given. Contents of major elements and S were determined by a chemical analysis; REE, by ICP AES; Ag, by AAS; and the rest impurity elements, by XRF.

Table 2. Isotope composition of sulfur in minerals of sulfide ores

Sample	Sulfide ore occurrence	Type of ores, mineral	$\delta^{34}S$, ‰
D-5-96	Ol'gino zone	Massive and disseminated pyrrhotite ores in schists, pyrite and pyrrhotite	5
7071			1.2
S-125-95			4.4
3060	Nizhnyaya zone	Massive sulfide ores, pyrite and pyrrhotite	2.8
3062			3.3
N-75		Carbonate–clay schists, pyrite	–21.5
3-58	Il'chir site (Ospa Formation (Il'chir unit?))	Black schists with disseminated pyrite mineralization	–17
348-1			–18.9
339			–13.6
9			–14.8
I-8		Sulfide ores in black schists, pyrrhotite	0.5
		Sulfide ores in black schists, pyrite	1.1
		Sulfide ores in black schists, pyrite	3.8
Er-131	Er'e–Khara-Zhalga site	Sulfide ores in black schists, pyrrhotite	–9.1
		Sulfide ores in black schists, pyrite	–8.4
Bg-498	Barun-Gol site	Sulfide ores in black schists, pyrite	–20.9

Quartz is characterized by $\delta^{18}O$ = 14.8 and 19.9‰ (Table 3). Calculation of the isotope composition of equilibrium fluid at 500 ºC yielded $\delta^{18}O$ = 12.2 and 17.3‰, respectively. These values are typical of metamorphogenic waters.

Gold contents in ores. Since gold is extremely unevenly distributed in the sulfide ores, we studied several 50 g specimens by a fire assay test and calculated the average gold content. The analyses were carried out for large (25–30 kg) trench samples. Chemical spectral analyses of small chip samples were performed with 10 g specimens and revealed ≤0.6 ppm Au. Hence, the applied technique of analysis of large samples permitted us to evaluate the true average contents of gold in the ores and to prove the presence of gold in pyrite–pyrrhotite ores. The gold contents determined in the sulfide ores by the above fire assay technique are within 0.1–4.4 ppm, averaging 1.48 ppm. Quartz contains 1.25 ppm Au (Table 4). The silver contents in the ores are also high, 2.5–12.0 ppm (Table 1).

Twenty-five grains of native gold were separated from crushed sulfide ores. The grains are 0.15 × 0.15 to 0.4 × 0.5 mm in size, goldish-yellow, and irregular-shaped (lumpy to platy, slightly elongate), with thin iron hydroxide films. Most grains are of high fineness, 884–992‰ (Fig. 10). Few particles are of low fineness; they vary in composition from native silver via kustelite (248–356‰) and electrum (500‰) to low- and medium-fineness gold (702‰). Sometimes, native gold has an impurity of Cu (few tenths of percent); single grains contain copper gold (Cu = 4.87–9.43 wt.%).

Table 3. Oxygen isotope composition of quartz

Sample	$\delta^{18}O$, ‰	$\delta^{18}O$ of fluid at 500 °C, ‰
D-16-96	+14.8	+12.2
D-26-96	+19.9	+17.3

Thus, the studied pyrrhotite ores are enriched in gold: Au = 2.5–12.0 ppm; average is 1.48 ppm (1.25 ppm in quartz veins). However, gold is extremely unevenly distributed in the ores, which often leads to a wrong evaluation of its content. The presence of Au and Ag mineral phases indicates that the ores are gold-bearing. The large masses of sulfide bodies and the wide spread of similar sulfide ores in southeastern East Sayan point to their commercial significance.

FORMATION CONDITIONS

Mineral thermobarometry. The *P–T* conditions of schist metamorphism were determined with mineral geothermometers based on analysis of the chemical compositions of rock-forming minerals. Calculation with the garnet–biotite geothermobarometers (Thompson, 1976; Holdaway and Lee, 1977) yielded the following values: T = 455 ºC, P = 4.96 kbar. Similar formation conditions are established from the *P–T* trends calculated with the garnet–clinopyroxene (Krogh, 1988) and muscovite–biotite (Hoisch, 1989) geothermometers. In the former case, a pressure of 5 kbar corresponds to a temperature of 543 ºC, and in the latter, to a temperature of 430 ºC. Calculation with the chlorite–muscovite geothermometer (Kotov, 1975) yields 450 ºC.

According to the phase diagram of the Fe–As–S system (Kretschmar and Scott, 1976) used as the arsenopyrite geothermometer, the triple point of the arsenopyrite, pyrite, and pyrrhotite coexistence corresponds to 491 ºC. The electrum–sphalerite geothermometer (Moloshag, 2009), based on the determination of Ag content (N_{Ag}) in electrum and Fe/(Fe + Mg) (X_{Fe}) in sphalerite, yielded a temperature of 446 ºC. The high X_{Fe} value of sphalerite is indirect evidence for the high-temperature conditions of its formation.

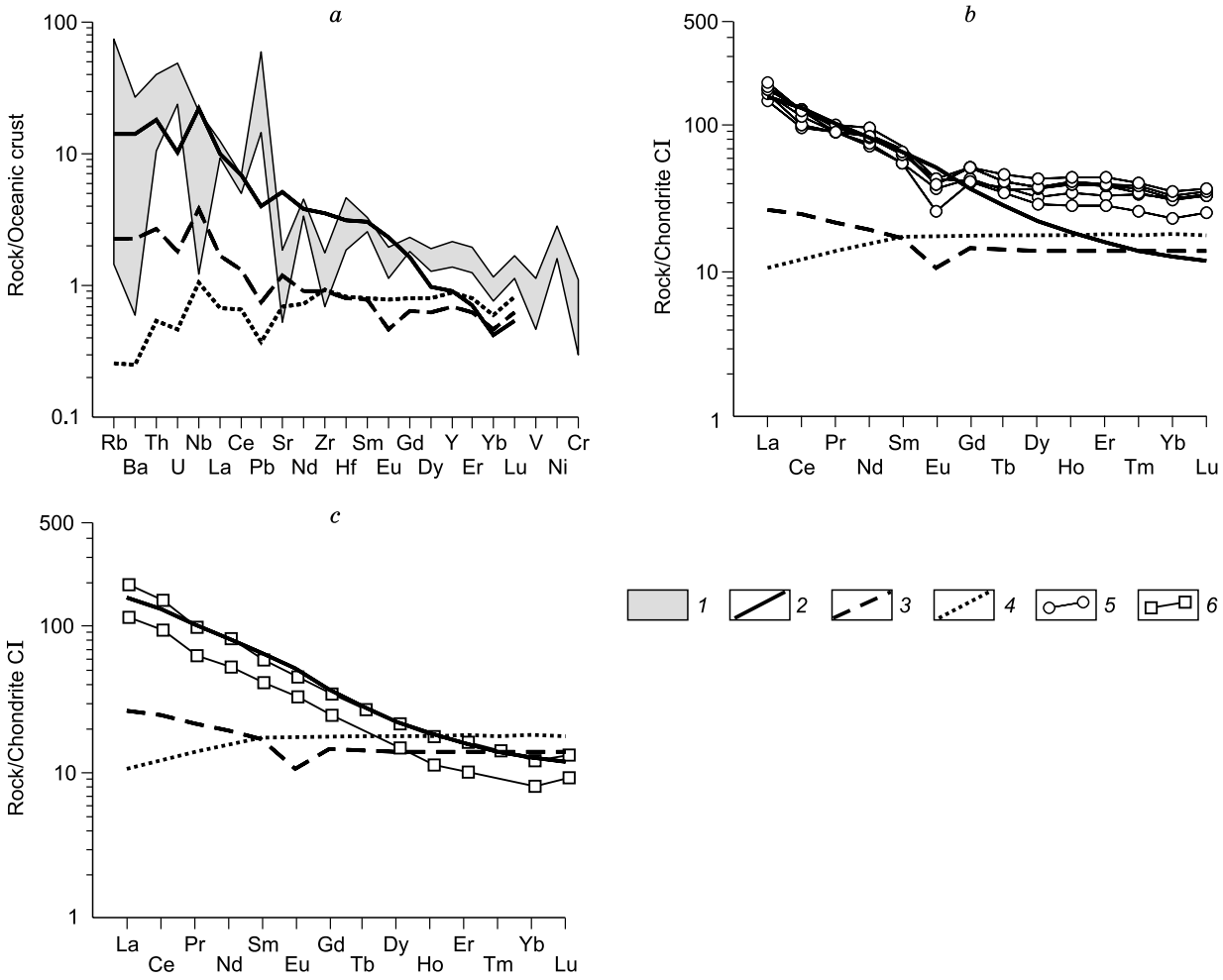

Fig. 8. Spidergram (*a*) and REE patterns of sulfide ores (*b*) and the host schists (*c*). *1,* composition field of sulfide ores; *2*, REE pattern of OIB; *3*, REE pattern of E-MORB; *4*, REE pattern of N-MORB; *5*, REE patterns of sulfide ores; *6*, REE patterns of the host schists.

Thus, the temperatures estimated with ore mineral geothermometers correspond to the formation temperatures of metamorphic silicate minerals. This permits a more reliable estimation of the *P–T* conditions of rock metamorphism: 430–540 ºC and ~5 kbar. These conditions correspond to the lower boundary of the epidote–amphibolite facies of metamorphism (Dobretsov et al., 1970) and are confirmed by the presence of typomorphic minerals of this facies (garnet, hornblende, epidote, etc.) in the assemblages of rock-forming minerals. Since similar formation conditions were established from the compositions of ore minerals, the latter might have been redeposited during metamorphism. In particular, the appearance of arsenopyrite metacrysts and electrum and native-gold particles and the high X_{Fe} values of sphalerite are due to metamorphism of primary sulfide ores.

The structures and textures of the studied rocks and ores testify to the redeposition of ore material with the participation of a fluid phase, whose presence is confirmed by the appearance of quartz lenses, veins, and veinlets subconformable with the bedding of the schist strata and framed by sites with hydrous minerals (sericite, biotite, amphiboles, and epidote). The transfer of ore-forming components by fluids was also reported by Ohmoto (1996). The presence of metamorphogenic fluid might have influenced the coarsening of native-gold particles.

To elucidate the composition of the fluid phase and to refine the *P–T* conditions of ore formation, we performed a thermobarogeochemical study of FI in quartz veins in the sulfide bodies.

Thermobarogeochemical study. Three varieties of FI have been recognized in the studied quartz grains: (1) primary, present as single inclusions or forming small groups (3 to 5–7 inclusions) outside of the healed cracks; (2) primary–secondary, forming chains within the mineral grains; and (3) secondary, localized in the healed cracks cutting the borders of the grains. The genesis of secondary and primary–secondary inclusions is unclear and thus was not studied.

More than 40 primary FI were studied in quartz and siderite from quartz veins, but not all of their parameters were reliably determined because of the very small size of some

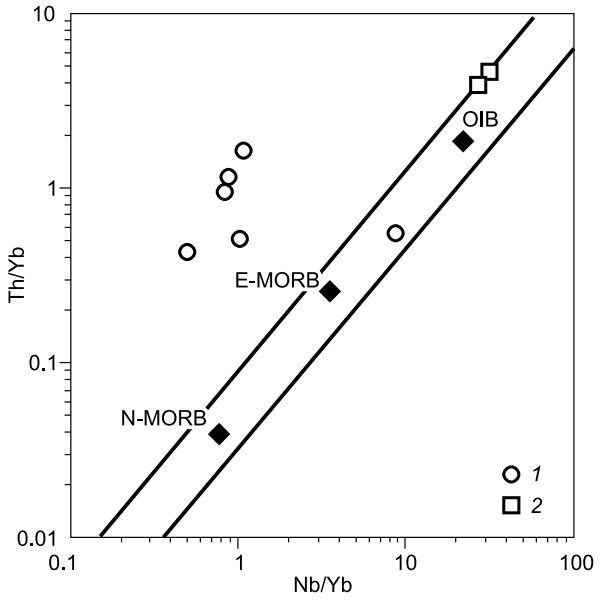

Fig. 9. Th/Yb–Nb/Yb diagram with the composition points of sulfide ores (*1*) and the host amphibole schists (*2*). Lines mark the compositions of N-MORB, E-MORB, and OIB.

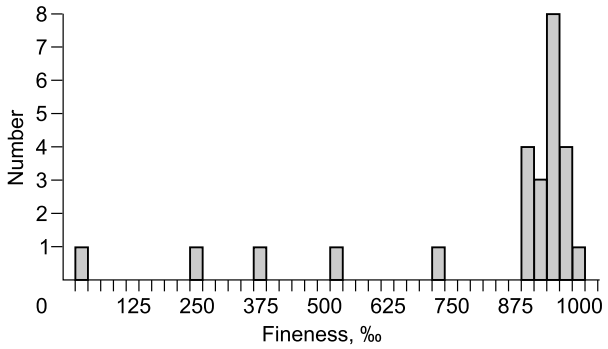

Fig. 10. Histogram of the fineness of native gold from sulfide ores (constructed from analytical data on 25 gold particles).

inclusions. The FI are of essentially aqueous ($L_{H_2O} \geq G >$ Crystal) and essentially gas ($G > L_{H_2O}$) types (Fig. 11). They are seldom larger than 10–12 μm (mostly, 3–8 μm), which significantly hampers thermometric experiments. Solid phase is present in all essentially aqueous inclusions and is somewhat smaller than the gas bubble (Fig. 11*a–f*); this size proportion is constant, which gives grounds to regard the solid phase as a daughter phase. Many quartz grains contain both homogeneous inclusions and syngenetic essentially aqueous and essentially gas FI within the same growth zone (Fig. 11*d–h*), which indicates local heterogenization (boiling) of the mineral-forming fluid. Such syngenetic inclusions are also observed in xenomorphous siderite grains (Fig. 11*j–l*) from later formed carbonate veinlets. The inclusions in siderite are very small (mostly ≤3–4 μm); therefore, they were not always appropriate for thermometric experiments.

Table 4. Results of fire assay test of trench and chip samples from the Ol'ginskoe ore occurrence

Sample	Number of 50 g specimens	Calculated Au content, ppm	Sampling interval thickness, m	Au content from chemical spectral analysis data, ppm	Sample description
D-1-96	4	0.35	1.3	B.d.l.	Biotite–garnet–amphibole–quartz schists
D-2-96	4	0	1.0	0.04	Amphibole–garnet schist
D-3-96	4	0.2	1.0	0.01	Plagioclase–biotite–amphibole schists with pyrrhotite
D-4-96	12	0.67	1.0	0.0025	Amphibole schist with pyrrhotite
D-5-96	12	2.0	1.5	0.015	Pyrrhotite ore with intercalates of carbonaceous quartz material
D-6-96	12	1.13	1.0	0.004	Quartz–pyrrhotite ores with chalcopyrite (30–45%)
D-7-96	12	2.11	1.0	0.015	Carbonaceous pyrrhotite ores (40–60%) with chalcopyrite (1–2%) and arsenopyrite
D-8-96	6	0.2	1.0	B.d.l.	Pyrrhotite ores (40–60%) with scarce chalcopyrite and intercalates of carbonaceous quartz material
D-9-96	4	1.0	1.0	B.d.l.	Pyrrhotite ores (40–60%) with scarce chalcopyrite and intercalates of carbonaceous quartz material
D-10-96	4	0.45	1.0	0.03	Pyrrhotite ores (40–60%) with scarce chalcopyrite and intercalates of carbonaceous quartz material
D-16-96	10	1.25	0.5	0.0045	Yellowish transparent coarse-crystalline quartz with nests (3–5 cm), veinlets, and inclusions of pyrrhotite
D-18-96	12	2.15	0.2	0.06	Fine-grained pyrite–pyrrhotite ores with scarce arsenopyrite crystals
D-19-96	12	0.1	0.2	0.012	Fine-grained pyrite–pyrrhotite ores with scarce arsenopyrite crystals
S-26-96	4	4.4	–	B.d.l.	Submicrocrystalline pyrrhotite ore with bands of medium-grained pyrrhotite

Note. Fire assay test was carried out at the Republican Analytical Center State Enterprise, Ulan Ude, and chemical spectral analysis, at the Geological Institute, Ulan Ude. B.d.l., below detection limit (<0.002 ppm).

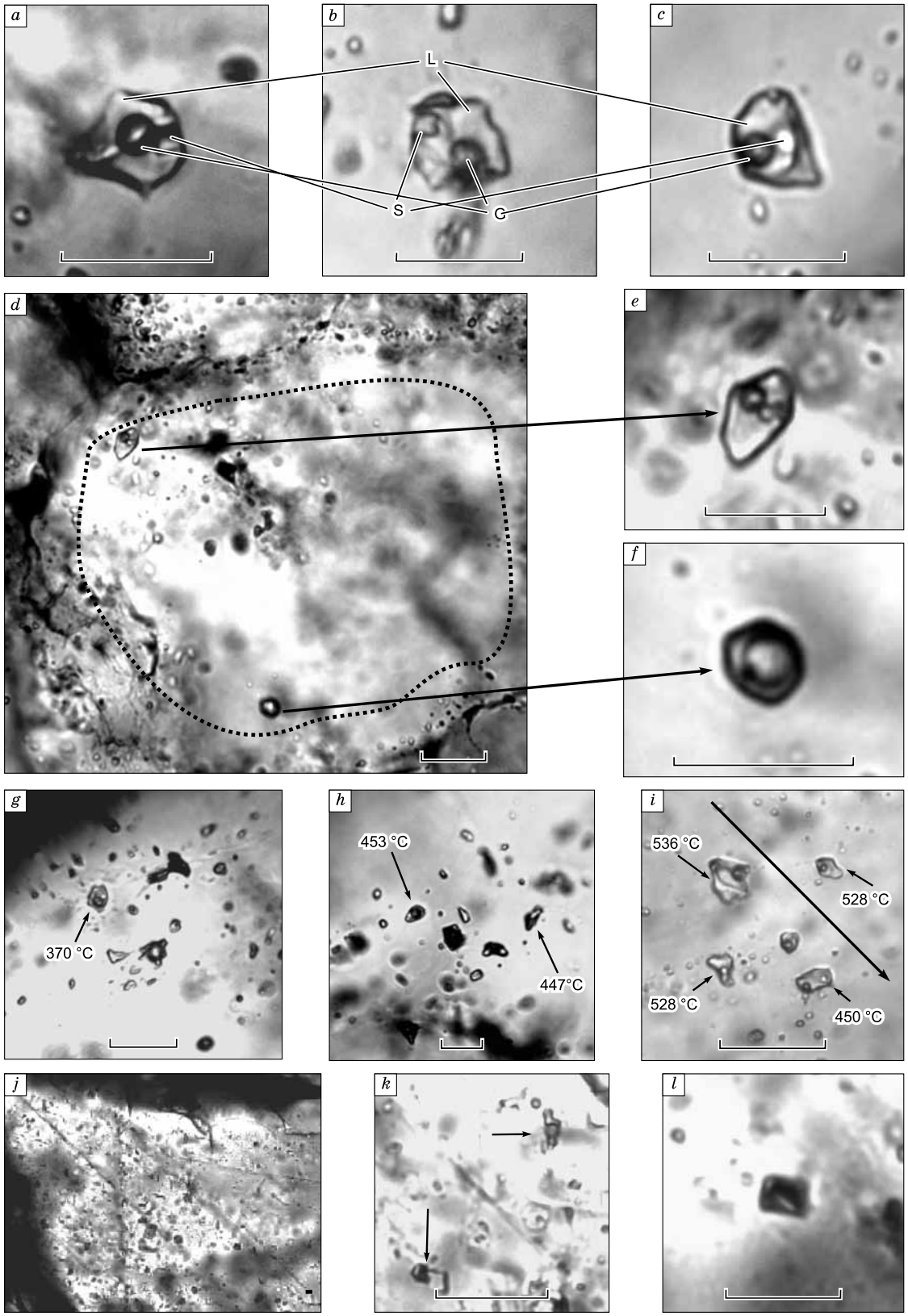

Fig. 11. Morphology of fluid inclusions in quartz. *a–c*, Three-phase FI in quartz; *d*, quartz grain with syngenetic essentially hydrous (*e*) and essentially gas (*f*) FI from the same growth zone (dashed line); *g*, *h*, quartz grains containing groups of essentially hydrous and essentially gas FI (arrows show the homogenization temperatures of FI); *i*, group of FI (arrow shows the direction from core to edge of quartz grain); *j*, carbonate (siderite) grain with FI: essentially hydrous (*k*) and essentially gas (*l*). Hereafter, L, aqueous solution, G, gas phase, S, solid phase. Scale bar 10 μm.

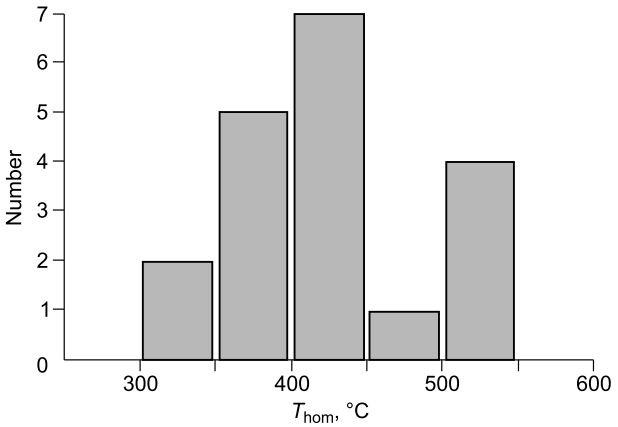

Fig. 12. Histogram of the homogenization temperatures of FI.

The measured homogenization temperature (T_{hom}) of primary inclusions in quartz varies from 340 to 536 ºC, with most of the values falling in the range 400–450 ºC (Table 5, Figs. 11*g–i* and 12). From core to edge of the grains it decreases by almost 100 ºC (Fig. 11*i*), which indicates the deposition of quartz under fluid temperature decrease. Siderite grains are characterized by lower homogenization temperatures of FI (370–440 ºC). According to the measured eutectic temperatures (T_{eut} = –35 to –37 ºC), Mg, Fe, and Na chlorides are major salt components of FI (Table 5). The solid phase of FI is presumably halite (NaCl), judging from its cubic crystals and the refraction index close to that of the host mineral (quartz). Daughter crystals dissolved at 11 to 225 ºC. On cooling of the inclusions, daughter phases again appeared. The melting point of the solid phase indicates the solution salinity of 26–33 wt.% NaCl equiv. (Table 5).

Knowing the salt composition of FI and the temperature of their trapping, we can estimate the maximum pressures of the two-phase field of fluid in the phase diagram of the water–chloride system. Figure 13 shows the *P–T* projections of critical curves (Steele-MacInnis et al., 2015) for some chloride systems established by thermobarogeochemical methods. For the most typical temperature of 450 ºC, we obtained the pressure range 400–500 bars for the systems $FeCl_2$–H_2O, NaCl + KCl–H_2O, and $MgCl_2$–H_2O. For temperatures from 340 to 536 ºC, we observed a wider range of pressures,

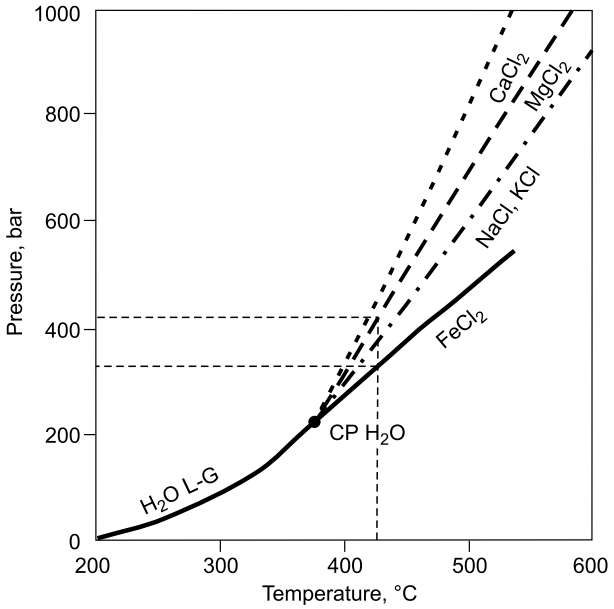

Fig. 13. *P–T* projections of critical curves for aqueous chloride solutions (Steele-MacInnis et al., 2015). CP, critical point of water.

~200–800 bars, depending on the type of salt system. Note that we obtained the maximum possible pressures for the heterogeneous field of fluid at these temperatures, which are probably not true but permit an approximate estimation of the mineral formation pressures. With the average T_{hom} = 424 ºC, we obtain the pressure range ~315–415 bars for different water–salt systems. This range is taken as the average pressure during the formation of quartz veins. These values differ considerably from the pressures during metamorphism, which evidences that quartz was deposited under drastic pressure decrease but at constant temperatures.

The presence of syngenetic essentially aqueous and gas FI in quartz indicates that they were trapped during the fluid heterogenization under conditions corresponding to the two-phase field of salt solution. Indeed, according to the *P–T* projection of the phase diagram of the system NaCl–H_2O, the estimated *P–T* conditions of FI trapping correspond to the field of heterogeneous fluid bounded by the upper critical curve and the three-phase (L + G + S) equilibrium curve (Fig. 14).

Table 5. Summary table of the results of thermobarogeochemical studies of primary FI

Phase composition of FI	T_{eut}	$T_{m\,sol}$	T_{hom}	T_{decr}	Salinity, wt.% NaCl equiv.	Salt system
	ºC					
G–L–S	–35 to –38	11–225	348–536	225–528	26.4–33.0	$FeCl_2$–H_2O $FeCl_3$–H_2O $MgCl_2$–NaCl–H_2O NaCl–$FeCl_2$–H_2O

Note. T_{eut}, eutectic temperature, $T_{m\,sol}$, melting point of the solid phase, T_{hom}, homogenization temperature of FI, T_{decr}, decrepitation temperature of FI.

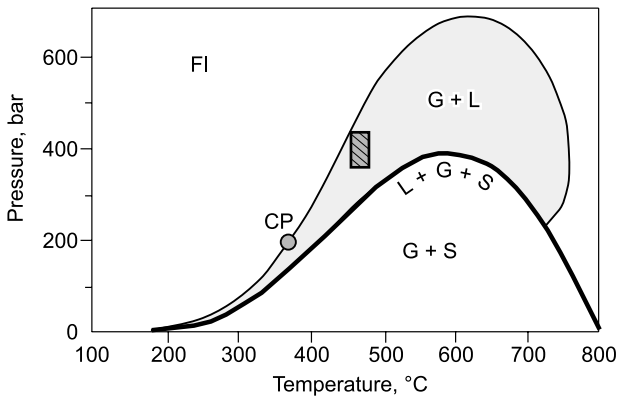

Fig. 14. *P–T* projection of the NaCl–H_2O phase diagram (Bodnar and Vityk, 1994). Hatched rectangle marks the approximate field of trapping of the studied FI. CP, critical point of water, Fl, field of homogeneous supracritical fluid.

DISCUSSION

The studied gold-bearing pyrrhotite ores are associated with volcanosedimentary deposits, basalt products with an impurity of siliceous and carbonaceous rocks, present in the ophiolite section. Sulfide bodies are conformable in bedding with the host rocks; the mineralization is controlled by lithology. The bodies are stratiform, form beds and lenses, and are rather extensive (up to a few kilometers). The ores contain relics of primary detrital structure and show no hydrothermal wallrock alterations. All these features indicate the synchronous formation of the sulfide bodies and the host volcanosedimentary deposits.

The ores are carbonaceous siliceous garnet–biotite schists enriched in sulfide minerals, mostly pyrrhotite, and containing impurities of other silicate minerals—tremolite, chlorite, albite, plagioclase, diopside, and epidote. As a result, the ores have high contents of S (10.49–17.8 wt.%) and SiO_2 (33.00–55.60 wt.%). Many rock-forming minerals of the schists have a Mn impurity, and garnet is represented by a Mn-containing variety, spessartine. The bulk content of MnO in the ores reaches 5 wt.%. The ore schists are similar in geochemistry to suprasubductional basalts of back-arc spreading zones (Pearce and Stern, 2006; Metcalf and Shervais, 2008). The content of Al_2O_3 in most samples is within 3–5 wt.%, but in some samples it reaches 11 wt.%, being close to those in MORB (Gale et al., 2013). Thus, the primary rocks were a mixture of volcanoclastic and basaltic volcanic rocks and siliceous deposits, with high contents of Fe sulfides and Mn minerals (probably, as Mn crusts) and with carbonaceous material. That is, these rocks are nearly identical in composition to hydrothermal deposits in mid-ocean ridges and back-arc spreading zones, which are products of "black smoker" discharge (Bogdanov et al., 2006).

According to the estimated *P–T* conditions of formation of the host schists, the degree of their metamorphism reached the base of the epidote–amphibolite facies (450–500 ºC, ~5 kbar). The wide variations in the degree of metamorphism at local sites testify to its dislocation type, which is due to the location of the volcanosedimentary strata in the basement of the ophiolite nappe. Dynamic metamorphism was responsible for the high dispersion of sulfide ores and the wide spread of ovoids of dark quartz and carbonaceous flints in them. Thermobarogeochemical studies have shown the lower pressures of quartz crystallization (a few hundred bars) and the temperatures of mineral formation close to the temperatures of metamorphism. This indicates that quartz veins formed under drastic pressure decrease. Such conditions arise in open cavities resulted from tectonic deformations.

Metamorphism was accompanied by transformation of ore minerals, in particular, pyrrhotitization of pyrite and release of impurity components. According to the phase diagram of the system Fe–As–S, the pyrite–pyrrhotite transition takes place at 491 ºC (Kretschmar and Scott, 1976); in the presence of carbonaceous material, the temperature of this transition decreases to ~200 ºC (Hall, 1986). The above estimated *P–T* conditions of metamorphism of sulfidized schists correspond to the conditions of the pyrite–pyrrhotite transition in the presence of carbonaceous material. Hence, during the metamorphism, pyrite underwent pyrrhotitization caused by the influence of both temperature and pressure and by the presence of carbonaceous material decreasing the pyrite–pyrrhotite transition temperature. According to the experimental data (Tomkins, 2010), this process runs by the reaction

$$2H_2O + C + 2FeS_2 \text{ (pyrite)} =$$
$$CO_2 + 2H_2S + 2FeS \text{ (pyrrhotite)}.$$

As a result, the released sulfide sulfur and carbon dioxide pass into a metamorphogenic fluid. At the beginning of metamorphism, pyrite grains are in equilibrium with small portions of aqueous H_2S solution and newly formed pyrrhotite (Fig. 15*a*). An increase in the degree of metamorphism leads to the release of water bound in hydrous minerals and to the complete pyrrhotitization of pyrite with the release of water and H_2S, which, in turn, results in a S-containing fluid phase (Fig. 15*b*). The latter is likely to be responsible for the low sulfur content in pyrrhotite. In addition, pyrrhotitization of pyrite leads to the release of impurity elements and the formation of new sulfide mineral phases: metacrysts of Ni–Co-containing arsenopyrite and fine and small microinclusions of galena and sphalerite in pyrrhotite. Gold shows similar behavior. After the release during the pyrite–pyrrhotite transition, its particles coarsen up to 1.0–1.5 mm. An experimental study of this process (Kalitkina et al., 1971) showed the appearance of gold particles when pyrite with invisible gold is replaced by pyrrhotite. Coarsening of native-gold particles during metamorphism was also revealed in pyrite ores in the Urals, which are fragments of ancient submarine sulfide structures (Vikent'ev, 2004). Primary Mn minerals were almost completely transformed, and Mn en-

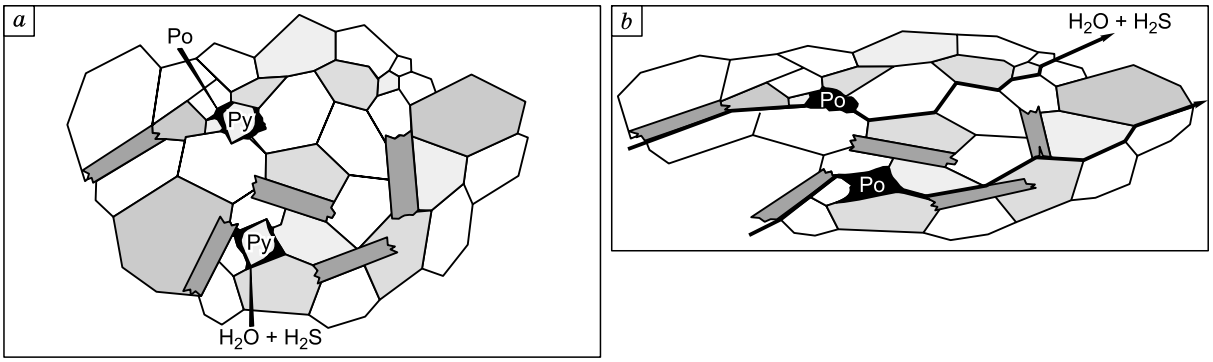

Fig. 15. Schematic model of pyrite pyrrhotitization during metamorphism depending on the degree of deformation (Tomkins, 2010). *a*, *b*, For explanation, see the text.

tered the structures of metamorphic silicate minerals (garnet, chlorite, epidote, etc.).

Since the above paleohydrothermal systems have the geochemical features of back-arc basalts and high contents of Pb, As, Au, and Ag, they can be regarded as the evolution products of the back-arc basin of the Dunzhugur island-arc system including the ophiolites under study. The $\delta^{34}S$ values of the sulfide ores vary from 0.5 to 5‰ and correspond to the sulfur isotope compositions of "black smoker" sulfides (Bogdanov et al., 2006; Seal, 2006), whereas the sulfides disseminated in the host schists and amphibolites and not present in orebodies have a light sulfur isotope composition ($\delta^{34}S$ = –8.4 to –21.5‰). Negative values of $\delta^{34}S$ are typical of sedimentary sulfide minerals formed through the intense fractionation of sulfur isotopes caused by bacterial or thermochemical reduction of seawater sulfates (Seal, 2006). Hence, the $\delta^{34}S$ values (0.5–5.0‰) of sulfides in the pyrite bodies indicate their formation from hydrothermal sulfur and accompanying ore-forming elements supplied with metal-bearing solutions.

The origin of Mn ores (so-called manganese crusts) is also related to the activity of submarine hydrothermal systems, often associated with sulfide structures (Bogdanov et al., 2006; Dubinin et al., 2008). The high contents of Mn in sediments are often the evidence for their deep-water formation. Therefore, the Fe/Mn ratio is used as a geochemical indicator in study of marine and oceanic bottom sediments.

Thus, the appearance of primary gold-bearing sulfide minerals is related to the evolution of submarine hydrothermal systems ("black smokers") in the back-arc spreading zone. For this reason, the studied mineralization can be referred to as a VMS (volcanogenic massif sulfide) deposit subjected to later metamorphism of the epidote–amphibolite facies. Such deposits are stratiform bodies of gold-bearing sulfide ores that settle out of hydrothermal solutions at the bottom of sea or ocean basins at the divergent plate boundaries (Barrie and Hannington, 1999; Galley et al., 2007). They occur among volcanosedimentary deposits and are usually coeval with volcanic rocks. It is believed that VMS deposits result from the hydrothermal mobilization of metals from oceanic crust (Sharman et al., 2015; Patten et al., 2016). They have high contents of base metals (Fe, Cu, Zn, and Pb) but can also be enriched in Au, Ag, As, Sb, Se, Te, and Bi, with their major ore minerals being pyrite, pyrrhotite, sphalerite, chalcopyrite, galena, and magnetite, respectively, present in different proportions (Galley et al., 2007). The deposits can be either gold-bearing or gold ore, depending on the degree of their gold enrichment. Gold-bearing deposits form at any gold-enriched sites of oceanic crust; most often, massive sulfide ores are produced within oceanic and incipient continental island arcs, rift arcs, and back-arc basins under lithospheric-plate stretching (Pitcairn, 2011; Webber et al., 2013). The contents of Au in recent submarine hydrothermal sulfide structures of back-arc basins vary from 3 to 15 ppm, with most of gold being invisible (Vikent'ev, 2004). Similar gold contents were probably specific to the primary sulfide deposits, whose metamorphism resulted in the pyrrhotite ores under study.

Ores of the Ol'ginskoe occurrence differ from ores of VMS deposits in low contents of Ba, Cu, Zn (hundredths of wt.%), and Au (average content is 1.5 ppm). The contents of these ore-forming elements in primary hydrothermal-sedimentary ores are unknown, but by analogy with recent deposits of submarine hydrothermal fields of back-arc spreading zones, the contents of Cu, Pb, Zn, and Ba can reach a few wt.% (Bogdanov et al., 2006) and the contents of Au are 3–15 ppm (Vikent'ev, 2004). This compositional difference can be for two reasons. First, submarine sulfide structures are usually zoned, and essentially pyrite ores of VMS deposits are the most mature: They resulted from reactions of primary (primitive) ores with late hydrothermal fluids. Probably, the schists have preserved only fragments of pyrite zones with a small impurity of complex metal sulfides. In this case, relics of the latter must have been found in numerous outcrops of a volcanosedimentary plate within the ophiolite belts in southeastern East Sayan.

Since no fragments of pyrite–polymetallic bodies were found in ophiolites, the most likely reason for the above compositional difference is the partial removal of ore-forming components from sulfide bodies during epigenetic trans-

formations of primary ores. As shown by Ohmoto (1996), Cu, Pb, Zn, Ba, and Ca can be removed and redeposited by older hydrothermal fluids in the course of the evolution of an underwater hydrothermal system during the formation of a sulfide structure, when fluids percolate through earlier sulfide deposits. Our research has revealed a fluid phase, but it formed through metamorphism processes during the obduction of ophiolite blocks. The oxygen isotope composition calculated for the fluid in equilibrium with quartz is typical of metamorphogenic waters ($\delta^{18}O$ = 12.2–17.3‰.), which agrees with the general geologic situation. This fluid was a highly concentrated salt (Fe, Na, and K chlorides) solution (26–33 wt.% NaCl equiv.) periodically boiling because of the pressure drop in the cavities, which led to the formation of quartz veins and veinlets. Despite the high contents of sulfur in the host substratum and, apparently, in the fluid, the quartz veins are extremely poor in sulfide minerals. This might be due to the high temperatures (>450–500 ºC) of quartz deposition. Since the solubility of S, Cu, and Zn increases with temperature (Huston, 1998; Duan et al., 2007), the ore components are dissolved in these conditions and are removed beyond the orebody. As shown earlier (Seward et al., 2014), Au, Pb, Cu, and Zn in hydrothermal solutions are transferred in the form of chloride or hydrosulfide complexes (Seward et al., 2014). The presence of chlorides in the fluid was established by cryometry, and the high saturation of the medium with sulfur suggests its presence in the solutions.

In the regional gold–sulfide–quartz deposits (Zun-Kholba, Vodorazdel'noe, Zun-Ospa, etc.), the orebodies bearing gold–polysulfide mineral assemblage with a predominance of pyrite, galena, sphalerite, and chalcopyrite often contain fragments and relics of primary stratiform sulfide ores similar to ores of the Ol'gino zone. This gives grounds to consider such hydrothermal-sedimentary sulfide ores to be at least one of major sources of gold and ore-forming components. This conclusion is based not only on the presence of sulfide body relics but also on the following facts:

(1) All gold–polysulfide mineral deposits in this region show similar sulfur isotope compositions, $\delta^{34}S$ = 2–6‰ (Mironov and Zhmodik, 1999; Zhmodik et al., 2008), corresponding to that of pyrrhotite ores;

(2) The deposits are localized in zones of intense tectonic dislocations (shears, thrusts, and melange zones), where the energy of tectonic processes causes the redistribution of material, including the transformation of primary sulfide bodies (Mironov and Zhmodik, 1999; Roshchektaev et al., 2000; Gordienko et al., 2016);

(3) Fe, Pb, Cu, and Zn are major ore-forming elements accompanying Au; these elements are typical of "black smoker" sulfide structures, which indicates that the components removed from primary metal-bearing sediments were redeposited in zones of tectonic deformations and formed gold-bearing mineralized zones and quartz vein bodies;

(4) the gold–sulfide–quartz deposits are younger than the metal-bearing sediments.

Dating showed the prolonged existence of an ocean basin, from >1035 to ~800 Ma. Accumulation of sediments, including metal-bearing ones, and their melting and destruction in subduction zones proceeded throughout the ocean basin life. The obduction of ophiolites with fragments of sulfide structures is dated at ~800 Ma (Kuzmichev, 2004). At that time, metal-bearing sediments underwent metamorphism and volcanosedimentary rocks altered into schists and amphibolites. The metamorphism processes transformed primary metal-bearing sediments into gold-bearing pyrrhotite ores, whose fragments are present within the East Sayan ophiolite belts.

CONCLUSIONS

(1) The geologic position, textures, structures, and mineral-geochemical and isotope parameters of the studied sulfide ores indicate their formation in submarine deep-water environments as a result of the activity of hydrothermal systems, analogs of "black smokers", that later underwent metamorphism.

(2) The estimated *P–T* conditions of metamorphism are ~5 kbar and 430–540 ºC, which corresponds to the boundary between the greenschist and epidote–amphibolite facies. The local occurrence of the studied mineral assemblages points to dynamic metamorphism of the sulfide-containing strata located in the base of the ophiolite nappe. The temperatures of formation of ore minerals are close to the above estimates.

(3) Quartz veins were formed by heterogeneous fluids with salinity of 26.3–33.0 wt.% NaCl equiv. in the temperature range 536–340 ºC and at rather low pressures of 170–520 bars. The main salt components of ore-forming solutions were Fe and Mg chlorides with a Na chloride impurity. The veins formed on the background of a slight temperature decrease and a drastic pressure drop caused by the appearance of open cavities as a result of tectonic deformations, which trapped a percolating metamorphogenic fluid.

(4) The low contents of gold and some ore-forming elements (Zn, Cu and Pb) in pyrrhotite ores indicate their removal with a metamorphogenic fluid. These ore-forming elements might have been the source of material for later gold deposits of the Urik–Kitoi zone in East Sayan.

This study was supported by grant 18-05-00489-a from the Russian Foundation for Basic Research.

REFERENCES

Barrie, C.T., Hannington, M.D., 1999. Classification of volcanic-associated massive sulfide deposits based on host-rock composition. Rev. Econ. Geol. 8, 1–11.

Belichenko, V.G., Butov, Yu.P., Boos, R.G., Vratkovskaya, S.V., Dobretsov, N.L., Dolmatov, V.A., Zhmodik, S.M., Konnikov, E.G., Kuz'min, M.I., Medvedev, V.N., Mironov, A.G., Postnikov, A.A., Sklyarov, E.V., Filimonov, A.V., Shafeev, A.A., 1988. Geology and Metamorphism of East Sayan [in Russian]. Nauka, Novosibirsk.

Bogdanov, Yu.A., Lisitsyn, A.P., Sagalevich, A.M., Gurvich, E.G., 2006. Hydrothermal Ore Genesis of the Ocean Bottom [in Russian]. Nauka, Moscow.

Bodnar, R.J., Vityk, M.O., 1994. Interpretation of microthermometric data for H_2O–NaCl fluid inclusions, in: De Vivo, B., Frezzotti, M.L. (Eds.), Fluid Inclusions in Minerals, Methods and Applications. Virginia Tech, Blacksburg, VA, pp. 117–130.

Borisenko, A.S., 1977. Study of the salt composition of solutions of gas–liquid inclusions in minerals by the cryometric method. Geologiya i Geofizika (Soviet Geology and Geophysics) 18 (8), 16–27 (11–19).

Budyak, A.E., Goryachev, N.A., Skuzovatov, S.Yu., 2016. Geodynamic background for large-scale mineralization in the southern environs of the Siberian Craton in the Proterozoic. Dokl. Earth Sci. 470 (2), 1063–1066.

Dobretsov, N.L., Reverdatto, V.V., Sobolev, V.S., Sobolev, N.V., 1970. Metamorphism Facies [in Russian]. Nedra, Moscow, Vol. 1.

Dobretsov, N.L., Konnikov, E.G., Medvedev, V.N., Sklyarov, E.V., 1985. Ophiolites and olistostromes of East Sayan, in: Riphean–Lower Paleozoic Ophiolites of Northern Eurasia [in Russian]. Nauka, Novosibirsk, pp. 34–58.

Dobretsov, N.L., Belichenko, V.G., Boos, R.G., Butov, Yu.P., Gordienko, I.V., Zhmodik, S.M., Ignatovich, V.I., Konstantinova, K.K., Kotkin, V.V., Kulikov, Yu.I., Lyuchkin, V.A., Mityukhin, E.N., Nemchinov, V.G., Osokin, P.V., Postnikov, A.A., Rasskazov, S.V., Roschchektaev, P.A., Sisykh, N.N., Sklyarov, E.V., Skopintsev, V.G., Shulyak, G.B., 1989. Geology and Ore Potential of East Sayan [in Russian]. Nauka, Novosibirsk.

Duan, Zh., Sun, R., Liu, R., Zhu, Ch., 2007. Accurate thermodynamic model for the calculation of H_2S solubility in pure water and brines. Energy & Fuels 21, 2056–2065.

Dubinin, A.V., Sval'nov, V.N., Uspenskaya, T.Yu., 2008. Geochemistry of the authigenic ferromanganese ore formation in sediments of the Northeast Pacific Basin. Lithol. Mineral. Resour. 43 (2), 99–110.

Faure, G., 1986. Principles of Isotope Geology. John Wiley & Sons, New York.

Fedotova, A.A., Khain, E.V., 2002. Tectonics of Southern East Sayan and Its Position in the Ural–Mongolian Belt [in Russian]. Nauchnyi Mir, Moscow.

Gale, A., Dalton, C.A., Langmuir, Ch.H., Su, Y., Schilling, J.-G., 2013. The mean composition of ocean ridge basalts. Geochem. Geophys. Geosyst. 14, 489–518.

Galley, A.G., Hannington, M.D., Jonasson, I.R., 2007. Volcanogenic massive sulphide deposits, in: Goodfellow, W.D. (Ed.), Mineral Deposits of Canada: A Synthesis of Major Deposit Types, District Metallogeny, the Evolution of Geological Provinces, and Exploration Methods. Geological Association of Canada, Mineral Deposits Division, Spec. Publ. 5, pp. 141–161.

Gordienko, I.V., Roshchektaev, P.A., Gorokhovsky, D.V., 2016. Oka ore district of the Eastern Sayan: geology, structural–metallogenic zonation, genetic types of ore deposits, their geodynamic formation conditions, and outlook for development. Geol. Ore Deposits 58 (5), 361–382.

Hall, A.J., 1986. Pyrite–pyrrhotine redox reactions in nature. Mineral. Mag. 50, 223–229.

Hoisch, T.D., 1989. A muscovite–biotite geothermometer. Am. Mineral. 74 (5–6), 565–572

Holdaway, M.J., Lee, S.M., 1977. Fe–Mg cordierite stability in high-grade pelitic rocks based on experimental, theoretical, and natural observations. Contrib. Mineral. Petrol. 63, 175–198.

Huston, D.L., 1998. The hydrothermal environment. J. Aust. Geol. Geophys. 17 (4), 15–30.

Kalitkina, N.A., 1971. Study of the processes of coarsening and disintegration of gold in pyrite and arsenopyrite. Vestnik MGU. Ser. Geol., No. 5, 107–110.

Khain, E.V., Bibikova, E.V., Kröner, A., Zhuravlev, D.Z., Sklyarov, E.V., Fedotova, A.A., Kravchenko-Berezhnoy, I.R., 2002. The most ancient ophiolite of the Central Asian fold belt: U–Pb and Pb–Pb zircon ages for the Dunzhugur complex, Eastern Sayan, Siberia, and geodynamic implications. Earth Planet. Sci. Lett. 199 (3–4), 311–325.

Kotov, N.V., 1975. Muscovite–chlorite paleothermometer. Dokl. Akad. Nauk SSSR 222 (3), 700–704.

Kretschmar, U., Scott, S.D., 1976. Phase relations involving arsenopyrite in the system Fe–As–S and their application. Can. Mineral. 14, 364–386.

Krogh, E.J., 1988. The garnet–clinopyroxene Fe–Mg geothermometer—a reinterpretation of existing experimental data. Contrib. Mineral. Petrol. 99, 44–48.

Kuzmichev, A.B., 2004. Tectonic History of the Tuva–Mongolian Massif: Early Baikalian, Late Baikalian, and Early Caledonian Stages [in Russian]. Probel-2000, Moscow.

Kuzmichev, A.B., 2015. Neoproterozoic accretion of the Tuva–Mongolian massif, one of the Precambrian terranes in the Central Asian Orogenic Belt, in: Kroner, A. (Ed.), Composition and Evolution of Central Asian Orogenic Belt: Geology, Evolution, Tectonics, and Models. Borntraeger Science Publishers, Stuttgart, pp. 66–92.

Kuzmichev, A.B., Larionov, A.N., 2013. Neoproterozoic island arcs in East Sayan: duration of magmatism (from U–Pb zircon dating of volcanic clastics). Russian Geology and Geophysics (Geologiya i Geofizika) 54 (1), 34–43 (45–57).

Metcalf, R.V., Shervais, J.W., 2008. Suprasubduction zone ophiolites: Is there really an ophiolite conundrum? In: Wright, J.E., Shervais, J.W. (Eds.), Ophiolites, Arcs, and Batholiths: A Tribute to Cliff Hopson. Geol. Soc. Am. Spec. Pap. 438, pp. 191–222.

Mironov, A.G., Zhmodik, S.M., 1999. Gold deposits of the Urik–Kitoi metallogenic zone (East Sayan, Russia). Geologiya Rudnykh Mestorozhdenii 41 (1), 54–69.

Mironov, A.G., Bakhtina, O.T., Zhmodik, S.M., Kulikov, A.A., Ochirov, Yu.Ch., Kulikova, O.A., 1999. New type of gold mineralization in stratiform pyrrhotite ores of East Sayan. Dokl. Akad. Nauk 364 (6), 798–801.

Moloshag, V.P., 2009. Using mineral compositions for estimation of the physicochemical conditions of formation of Urals pyrite ores. Litosfera, No. 2, 28–40.

Nemerov, V.K., Stanevich, A.M., Razvozzhaeva, E.A., Budyak, A.E., Kornilova, T.A., 2010. Biogenic sedimentation factors of mineralization in the Neoproterozoic strata of the Baikal–Patom region. Russian Geology and Geophysics (Geologiya i Geofizika) 51 (5), 572–586 (729–747).

Ohmoto, H., 1996. Formation of volcanogenic massive sulfide deposits: the Kuroko perspective. Ore Geol. Rev. 10, 135–177.

Patten, C.J.C., Pitcairn, I.K., Teagle, D.A.H., Harris, M., 2016. Mobility of Au and related elements during the hydrothermal alteration of the oceanic crust: implications for the sources of metals in VMS deposits. Mineral. Deposita 51, 179–200.

Pearce, J.A., Stern, R.J., 2006. The origin of back-arc basin magmas: trace element and isotopic perspectives, in: Christie, D.M., Fisher, C.R., Lee, S.-M., Givens, S. (Eds.), Back-Arc Spreading Systems: Geological, Biological, Chemical, and Physical Interactions. AGU Monograph 166, Washington, pp. 63–86.

Pitcairn, I.K., 2011. Background concentrations of gold in different rock types. Appl. Earth Sci. 120, 31–38.

Posokhov, V.F., Mironov, A.G., Utina, E.D., 1994. Rb–Sr study of the Zun-Kholba gold deposit (East Sayan), in: Yearbook 1994 [in Russian]. GIN SO RAN, Ulan Ude, Issue 1, pp. 11–13.

Roshchektaev, P.A., Mironov, A.G., Doroshkevich, G.I., Bakhtina, O.T., Minin, V.V., Maurishnin, E.C., Ananin, V.A., Zhmodik, S.M., Kulikov, A.A., Osokin, A.P., Shelkovnikov, M.F., Zelenyi, E.N., Yavirskaya, T.E., Morgunov, Yu.A., 2000. Gold of Buryatia. Book 1. Structure-Metallogenic Regionalization, Geologic Structure of Deposits, and Assessment of Resources [in Russian]. BNTs SO RAN, Ulan Ude.

Seal, R.R., 2006. Sulfur isotope geochemistry of sulfide minerals. Rev. Mineral. Geochem. 61, 633–677.

Seward, T.M., Williams-Jones, A., Migdisov, A., 2014. The chemistry of metal transport and deposition by ore-forming hydrothermal fluids, in: Holland, H., Turekian, K. (Eds.), Treatise on Geochemistry. Vol. 13: Geochemistry of Mineral Deposits. Elsevier, Oxford, pp. 29–57.

Sharman, E.R., Taylor, B.E., Minarik, W.G., Dube, B., Wing, B.A., 2015. Sulfur isotope and trace element data from ore sulfides in the Noranda district (Abitibi, Canada): implications for volcanogenic massive sulfide deposit genesis. Mineral. Deposita 50, 591–606.

Steele-MacInnis, M., Lecumberri-Sanchez, P., Bodnar, R.J., 2015. Synthetic fluid inclusions XX. Critical *PTx* properties of H_2O–$FeCl_2$ fluids. Geochim. Cosmochim. Acta 148, 50–61.

Thompson, A.B., 1976. Mineral reactions in pelitic rocks, II: Calculation of some *P–T–X* (Fe–Mg) phase relations. Am. J. Sci. 276, 425–454.

Tomkins, A.G., 2010. Windows of metamorphic sulfur liberation in the crust: Implications for gold deposit genesis. Geochim. Cosmochim. Acta 74, 3246–3259.

Vikent'ev, I.V., 2004. Formation Conditions and Metamorphism of Pyrite Ores [in Russian]. Nauchnyi Mir, Moscow.

Webber, A.P., Roberts, S., Taylor, R.N., Pitcairn, I.K., 2013. Golden plumes: substantial gold enrichment of oceanic crust during ridge–plume interaction. Geology 41, 87–90.

Zhmodik, S.M., Postnikov, A.A., Buslov, M.M., Mironov, A.G., 2006. Geodynamics of the Sayan–Baikal–Muya accretion–collision belt in the Neoproterozoic–Early Paleozoic and regularities of the formation and localization of precious-metal mineralization. Russian Geology and Geophysics (Geologiya i Geofizika) 47 (1), 187–201 (183–197).

Zhmodik, S.M., Mironov, A.G., Zhmodik, A.S., 2008. Gold-Concentrating Systems of Ophiolite Belts (by the Example of the Sayan–Baikal–Muya Belt) [in Russian]. Akadem. Izd. "Geo", Novosibirsk.

Editorial responsibility: A.S. Borisenko